MODELLING AND SIMULATION STUDY OF ELECTRO-THERMAL

CHARACTERISTICS AND EMITTED LIGHT CHARACTERISTICS IN SOLID

STATE INCANDESCENT LIGHT EMITTING DEVICES

A Thesis

by

ABHINAV SHUKLA

Submitted to the Office of Graduate and Professional Studies of
Texas A&M University
in partial fulfillment of the requirements for the degree of

MASTER OF SCIENCE

Chair of Committee,	Yue Kuo
Co-Chair of Committee,	Tahir Cagin
Committee Members,	Pao-Tai Lin
Head of Department,	Ibrahim Karaman

December 2020

Major Subject: Materials Science and Engineering

ABSTRACT

Recently, researchers have reported a unique solid state incandescent light emitting device (SSI-LED) made from a simple MOS capacitor with an amorphous high-k gate dielectric thin film deposited on the p-type Si substrate. Other than lighting applications, SSI-LED is promising candidate for on-chip optical interconnects and nonvolatile memories. The study of such devices can play a crucial role in their incorporation in future electronic and optoelectronic applications. In this thesis, the electrothermal characteristics of the SSI-LED is studied using finite element modeling in COMSOL Multiphysics program. Temperature distributions within and around individual nano-resistors of different sizes distributed randomly in the gate dielectric of SSI-LED were obtained with optimized boundary conditions. The current density variation near the edge of the large nano-resistors affected the local temperature distribution across the cross-section of nano-resistors.

The light filtration effect of ITO and a-Si:H thin films on the broad-band light emitted from the ZrHfO high-k dielectric based SSI-LED has been theoretically investigated and compared with the experimental observations. The deviation in peak wavelengths of computed spectra from experimental emission spectra suggested that the thin film filters above nano-resistors formed in the dielectric film might have a change in phase owing to the intense Joule heating during the passage of a large current. The broadband light spectrum emitted from the SSI-LED could be narrowed down with the

addition of thin film filters, and the peak of the new spectrum was dependent upon the optical properties of the material of the filter.

Light intensity distributions from nano-resistor based SSI-LED are also studied using physics-based analytical calculations. The inter-nanoresistor distance affected the resolvability of individual nano-resistor light sources. Formation of nano-resistor clusters and the presence of few large nano-resistors resulted in bright radiation spots observed at higher magnifications. Light from individual nano-resistors could not be resolved at lower magnifications. The device's center region was brightest, with light intensity diminishing uniformly in the radially outwards direction. The geometrical layout of the nano-resistors formed in the SSI-LED also affected the local light intensity distribution at higher magnifications.

DEDICATION

To my beloved late grandmother whom I lost during my master's

studies, my grandfather, my mother Pushpa Shukla, father Rajesh Kumar Shukla, and

brother Anchit Shukla

ACKNOWLEDGEMENTS

First and foremost, I wish to express sincere thanks to my advisor Dr. Yue Kuo for being generous and giving me the opportunity to work under his tutelage during my graduate study at Texas A&M University. Through his persistent training, guidance, and vast knowledge in semiconductors, I have learned extensively. His passion and work ethic towards research is extraordinary and has fostered scientific creativity and innovation. His constant encouragement and patient advice on academic and non-academic fronts have been paramount in completing this work.

I would also like to express my sincere appreciation to Dr. Tahir Cagin and Dr. Pao-Tai Lin for kindly agreeing to serve as my committee members and offering valuable inputs during my Master's study and research.

I owe special thanks to my colleagues in Thin Film Nano & Microelectronics Research Laboratory, Jia Quan Su, Wen-Shan Lin, and Lingguang Liu for the enormous support on my research work and the friendship beyond the academic life. There are numerous friends whom I cannot list for fear of missing some of them out. They were the ones I looked to for the courage to push through in difficult times. Thank you all for the support and the long-lasting memories I wish to cherish forever,

Finally, thanks to my parents, to whom I owe everything. Thank you for instilling in me the love for learning and knowledge and allowing me to pursue my goals.

CONTRIBUTORS AND FUNDING SOURCES

Contributors

This work was supervised by a thesis committee consisting of Professor Yue Kuo (advisor), Professor Tahir Cagin of the Department of Materials Science and Engineering, and Professor Pao-Tai Lin of the Department of Electrical and Computer Engineering.

All the work for the thesis was completed by the student independently.

TABLE OF CONTENTS

LIST OF FIGURES

LIST OF TABLES

1. INTRODUCTION AND LITERATURE REVIEW

1.1. Review on Light Emitting Devices

1.1.1. Conventionally Used Light Emitting Devices

Incandescence was first demonstrated from a heated wire in 1761. The filament based incandescent light bulb that emits white light when heated to a high temperature by passing electric current through it was first patented in 1904.[1] Incandescent lights have a great ability to render color and the color rendering index (CRI) for an incandescent bulb with a color temperature of 2700 K is a perfect 100, same as that of the sun.[2] Even though they are cheap to manufacture, an average incandescent bulb has a low lifespan of about 1200 hours and most of the energy consumed goes into heat with typically 5% or less converted into visible light (~10-20 lm/W). According to the most recent data by the Energy Information Administration, lighting alone is responsible for 8% of the residential and commercial electricity consumption in the U.S. The introduction of federal efficiency standards has led the transition to the use of compact fluorescent lamps (CFLs) and light emitting diode (LED) bulbs in recent years at the expense of inefficient incandescent light bulbs. Typical fluorescent lamps convert approximately 22% of the power input into visible light (~71 lm/W) and last 10 to 20 times longer when compared to an incandescent light bulb of similar light output.[3] Fluorescent light bulbs working principle is based on inelastic collisions of electrons with mercury atoms, which produce short-wave ultraviolet (UV) photons that further get converted into visible light by UV excitation of the fluorescent coating on a lamp's glass envelope. Modern CFLs can have efficiency up to

100 lm/W. However, fluorescent lamps have issues due to inclusion of mercury and are treated as hazardous to the environment. Additionally, CRI values for fluorescent light lie between 62-80 and leave some room for improvement.

When compared with incandescent and fluorescent lamps, the light emitting diodes (LED) exhibit higher efficiency and require about 90% and 50% less electricity, respectively.[4] Moreover, LEDs with equivalent light output last 25 and 4 times longer than incandescent lamps and fluorescent lamps, respectively.[4] According to the reports, highly efficient LEDs have the capability to reduce lightning energy consumption in the U.S. itself by approximately 38% and can save up to ~$17 billion/year.[5] The first visible-spectrum (red) radiation was reported from forward-biased $Ga(As_{1-x}P_x)$ p-n junction by Nick Holonyak, Jr. and S. F. Bevacqua in 1962.[6] Thereafter, in 1972, the first yellow LED was invented and the brightness of red and red-orange LEDs was improved by a factor of ten, broadening the potential applications of LEDs.[7] The light emission in LEDs is based on the principle that when the p-n junction diode is forward biased, electrons from the conduction band recombine with holes from the valence band, producing photons of energy equal to the band gap energy given by following equation[8]:

$$hv = \frac{hc}{\lambda} \cong E_g \qquad [1.1]$$

where h is the Planck's constant of $6.626 \times 10-34$ J/s, v is the frequency of light, c is the speed of light of 3×108 m/s, λ is the wavelength of light, and E_g is the band gap energy. Most of today's commercial LEDs are made from different combinations of III-V semiconductor materials depending upon the required emitted wavelengths like, GaAlAs for red, AlInGaP for yellow-orange, InGaN for blue and green, etc.[9]

Typically, the electron-hole recombination process can be classified into two kinds: radiative and non-radiative recombination.

Radiative recombination is the reverse process of a photon's absorption. The process happens when an electron jumps down from the conduction band to the valence band and spontaneously emits a photon in the process. Radiative transition is more relevant to direct bandgap semiconductors, where the band-to-band transition does not involve multiple steps, as the minimum energy state in the conduction band lies directly above the maximum energy state of the valence band in the energy vs momentum diagram. The associated crystal momentum of electrons and holes is the same for both conduction and valence band, as shown in the Figure 1(b).[9] Some III-V materials such as InAs, GaAs are examples of direct bandgap semiconductor materials.[9]

Non-radiative recombination, on the other hand, involves indirect bandgap semiconductor materials, for which the valence band's maximum energy state occurs at a different momentum relative to the minimum energy state of the conduction band. The electron transition in such materials is facilitated by formation of intermediate donor states between the conduction and valence bands. Such states are introduced by the addition of impurities (dopants) and capture the electron locally to provide the required momentum shift and thus makes way for the recombination process. The momentum shift is associated with emission or absorption of phonons and often cause temperature changes in the crystal lattice. Non-radiative recombination processes include Auger recombination, surface recombination and recombination at defects[10]. Examples of indirect bandgap materials

include Ge, crystalline Si and AlP[9]. Figure 1(a) shows the energy vs momentum diagram of an indirect bandgap material.[9]
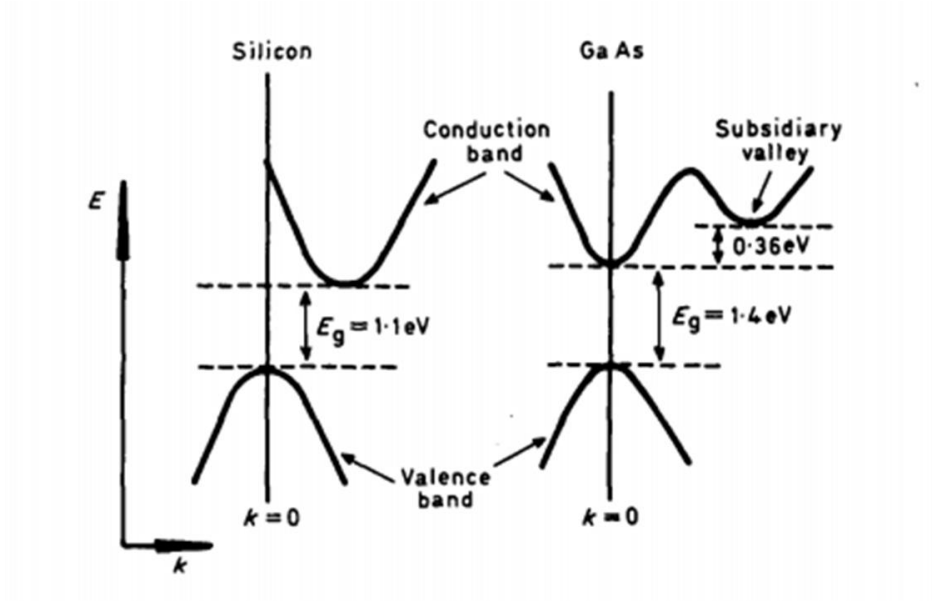
Figure 1. Band structures for (a) indirect bandgap (Si) and (b) a direct bandgap (GaAs) semiconductor. (Reprinted from Ref. 9. Copyright 1987 IERE.)

1.1.2. Towards White Light Emission

As discussed earlier, conventional p-n junction based LEDs emit photons of a single wavelength corresponding to the energy bandgap of the material. White LEDs, on the other hand, are quite different and are supposed to emit polychromatic light. There

have been multiple approaches to generate white light from LEDs. The first approach, a multi-LED approach, is used to generate white light by combining individual lights emitted from three primary coloured LED chips, i.e., red, blue, and green, as shown in Figure 2. The approach, however, requires controlled current supply to each of the three LEDs to generate appropriate white light.[11-13] The second approach, illustrated in Figure 3, uses an LED chip emitting ultraviolet (UV) light and a phosphor coating that absorbs the UV light, converting it to a broadband white light like the conventional fluorescent lamps discussed previously.[14] This method is less efficient as a large shift in wavelength (large Stokes shift) is required for the down-conversion of UV light[14]. A third approach for emission of white light follows a "partial conversion" concept and combines a phosphor coated blue LED chip with the green and red light emitted from phosphor[14], as shown in Figure 4. The phosphor partially absorbs the blue light from the LED chip, transmitting the rest of the blue light through. Therefore, a final combination of the blue light from the LED chip, green light from phosphor, and red light from phosphor together result in a white light. However, after it was reported that organic phosphors are not reliable under the harsh operating conditions of a blue LED, Shimizu et. al. suggested using an inorganic phosphor: Cerium-doped yttrium-aluminum garnet phosphor (YAG:Ce).[14-17] The approach, on further development, required only one LED chip run by single power source and is commercially the most successful, due to its efficiency and simplicity.[17] Even though LEDs are highly efficient, it is to be recognized that their fabrication involves complex process steps. For instance, the growth of hetero-epitaxy thin film layers is achieved using advanced systems like molecular beam epitaxy (MBE)

system or the highly toxic metal-organic chemical vapor deposition (MOCVD) apparatus.

Moreover, defect densities in the bulk film, and the crystal defects formed at interfaces as

a result of lattice mismatch during epitaxy, greatly affects the performance of such

LEDs.[18]
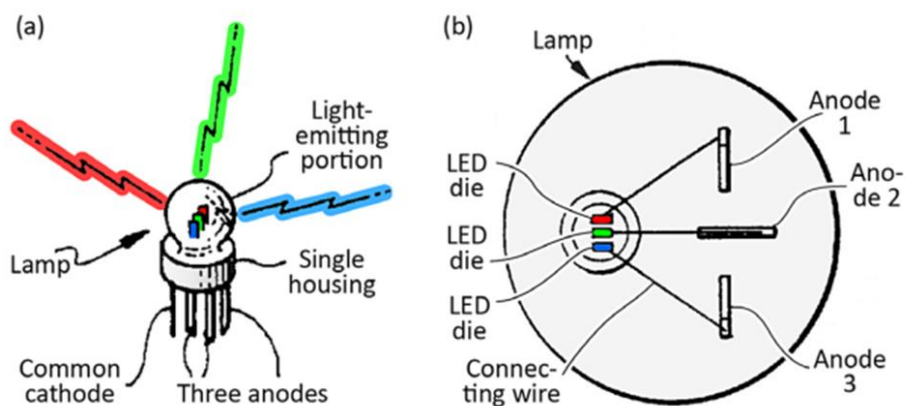
Figure 2. Multi-LED-chip white LED consisting of a red (R), green (G), and blue (B) LED chip (or die): (a) perspective view and (b) top view. Optical mixing of the RGB emission components results in white light. (Reprinted with permission from Ref. 14. Copyright 2017 Wiley.)
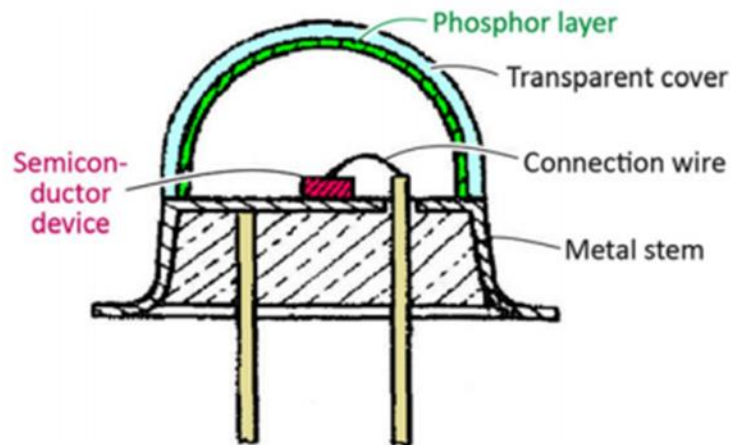
Figure 3. LED structure having an LED chip exciting a phosphor that is coated on the inside of a transparent cover. (Reprinted with permission from Ref. 14. Copyright 2017 Wiley.)
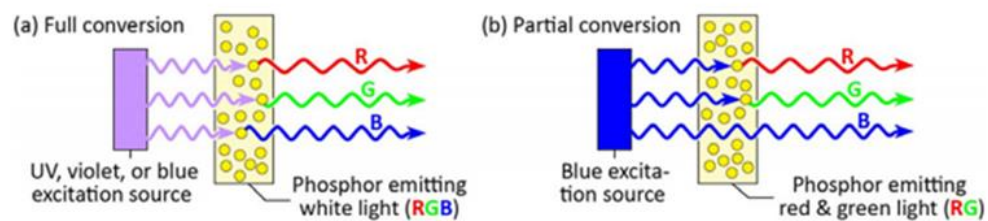
Figure 4. (a) Full conversion and (b) partial conversion of the excitation light in a white LED. (Reprinted with permission from Ref. 14. Copyright 2017 Wiley.)

Alternatively, quantum dots (QDs) are potential materials for the future LED industry and QD based LEDs have been used for white light emission, e.g., CdSe QD-

based white light LED.[19] However, in addition to being toxic to environment, CdSe QDs have low efficiency when used in white LEDs,[19] and poor CRIs (~71 for CdSe QDs)[20] when compared to incandescent lamps. Moreover, atmospheric exposures and operation under high electric fields tend to shorten the lifetime of QDs.[20] To overcome the above shortcomings, a more robust white light emitting device is required.

1.2. Solid State Incandescent Light Emitting Device

Recently, a novel single chip solid state-based light emitting device which is eco-friendly, simple to fabricate using current IC processes at low costs, and can emit broad band white light has been reported. The warm white light emission phenomenon from this device is like that of an incandescent lamp[21-29] and hence, it is referred to as the solid state incandescent light emitting device (SSI-LED). The light emission from the SSI-LED is attributed to the electromagnetic radiations generated by thermal excitation of the nano-sized conductive paths (or, nano-resistors), on passage of large currents through it. [21-29] During the Joule heating process, atoms in the nano-resistor get thermally excited, transferring some part of the kinetic energy to the electrons present in the lattice.[30] The excited electrons thus achieve higher energy states, and when these excited electrons jump back to lower energy states, the process is accompanied by photon emission corresponding to each of the transitions (relaxation)[30]. Due to near-continuum of electron energy states in solids, the resulting radiation is a continuous non-discrete spectrum.[30] The SSI-LED is made from a simple MOS capacitor with an amorphous high-k gate dielectric thin film, e.g., Zr-doped HfO_2 (ZrHfO), HfO_x, or WO_x deposited on the p-type Si

substrate.[21-29]. The light emission phenomenon occurs after the dielectric breakdown. A large number of permanent nano-resistors are formed due to the hard breakdown of the high-*k* dielectric thin film on application of large negative gate voltage, which also causes bump formation in the gate electrode[27]. The color correlated temperature (CCT) of the light emitted from the SSI-LED typically lies between 2,500 K and 4,500 K, and is the function of the gate voltage, dielectric material, and processing parameters.[25] Several studies have been done in the past to improve the SSI-LED electrical and optical properties by altering materials, structures, fabrication processes, etc. For instance, after deposition of the high-*k* dielectric film, an annealing step is usually carried out to reduce the defects in the film. The post-deposition annealing condition significantly affects the bulk- and interface-layer properties, which further changes the properties of nano-resistors formed, thereby affecting the emission characteristics of the SSI-LED.[25] The emitted light intensity from the SSI-LED can be enhanced by embedding nanocrystals, like ZnO and CdSe, in the gate dielectric layer.[21,27] A multilayer ZnO-HfO_x stack instead of a single layer HfO_x gate dielectric has also been used to intensify light emission.[31] The relative peak intensities of the SSI-LED are reported to increase from 3802.14 to 7777.19 (a.u.) for corresponding samples with one layer and three layers of ZnO-HfO_x films, respectively.[31] Other promising dielectric alternatives, like WO_2 and TiO_2, also reportedly enhanced light emission efficiency.[26,32] In addition to this, Si substrate dopant concentration affected the electrical and light emission characteristics of the SSI-LED composed of the HfO_x (16 nm)/ZnO (2 nm)/HfO_x (4 nm) stack sputter deposited sequentially. For example, light intensity reportedly increased 3 times on varying Si wafer's dopant concentration from

10^{14} cm^{-3} to 10^{18} cm^{-3} while the breakdown voltage decreased by 11%.[33] Furthermore, a MOS capacitor with co-planar structure has also been fabricated and demonstrated to emit light with similar optical characteristics, except at slightly higher intensities when compared to that of the conventional non-coplanar structured SSI-LED.[34]

Electrical properties of the nano-resistors formed in the device was studied in detail by Zhang et. al.[35] Various methods can be employed to estimate the effective resistance and Schottky barrier height of the nano-resistors using the SSI-LED's current-voltage (J-V) characteristics. The effective resistivities of all nano-resistors are reported to be about 499 Ω·cm, 551 Ω·cm, and 601 Ω·cm for the SSI-LED samples stressed at −20, −30, and −40 V gate voltages, respectively.[35] Moreover, the effective resistance of the nano-resistors increases from 150 Ω at 20 °C to 187 Ω at 60 °C for the -20 V stressed SSI-LED, indicating difference in nature of nano-resistors when compared to a conductor or a semiconductor.[35] The Schottky barrier height decreases from 0.60 eV to 0.56 eV with the increase of gate stress voltage from −20 V to −40 V at room temperature, respectively.[35] These important electrical parameters for the nano-resistors, in addition to certain assumptions, are utilized in this research for performing accurate modelling studies.

Various prospective applications of the nano-resistor devices have been reported so far. SSI-LEDs can emit light continuously for more than 20,000 hours in air without failure.[36] Other than the lighting application, the SSI-LED can be used as a light source for the on-chip optical interconnect system by depositing thin film filter layers, e.g., a multilayer stack of a-Si:H and SiN$_x$ films, on the top to narrow down the emitted broadband wavelength.[37,38] It also exhibits diode-like current-voltage (*I-V*) characteristics,

i.e., unidirectional current flow.[39] Furthermore, the device has a large "programmed" to "unprogrammed" leakage current ratio, making it a promising antifuse device, which is suitable for "one-time-programming" non-volatile memory.[39] Therefore, study of such a device can play a key role for its incorporation in future electronic and optoelectronic applications. At present, most of the studies done on SSI-LEDs have been experimental in nature and were focused towards understanding the operational behavior of this novel device. In this thesis, the authors employ computational techniques like Finite Element Analysis (FEA) to study the electrothermal characteristics of the device. Additionally, various fundamental physics-based analytical computations under certain assumptions are exploited as well to explain some of the experimental investigations.

1.3. Thesis Outline

Section 2 focuses on studying the electrothermal characteristics exhibited by the new solid state incandescent light emitting device. The physics-based mathematical model is formulated with governing equations and simulated using the COMSOL Multiphysics program. Temperatures within and around individual nano-resistors in different geometrical arrangements, distributions and sizes were calculated using finite element modeling. The temperature distribution across the complete device under various boundary conditions was simulated and optimized based on its optical emission spectrum. The results obtained are correlated with experimental data previously reported on the device and presented in detail.

11

Section 3 focuses on modeling the light emission spectra over the SSI-LED based on fundamental physical laws. The emission spectra from the thermal excitation of nano-resistors with and without inclusion of thin film filters like Indium Tin Oxide (ITO) or amorphous silicon (a-Si) are calculated and a comprehensive comparison with spectra measured from actual devices is presented. The light characteristics for the SSI-LED with ITO, a-Si and polycrystalline silicon (poly-Si) thin film filters are also discussed based upon their respective simulated emission spectrum.

Section 4 discusses the two- and three- dimensional light intensity distribution from the SSI-LED. The effect of inter nano-resistor distance on light source resolvability is investigated. Emitted light intensity distribution from randomly distributed nano-resistors at both high and low magnification is discussed in detail. The effects of geometrical layout of the nano-resistors formed in the SSI-LED on local light intensity distribution at higher magnifications is also studied.

Section 5 is the summary of various studies covered in the thesis and concludes the important outcomes.

2. SIMULATION STUDY OF ELECTROTHERMAL CHARACTERISTICS IN SOLID STATE INCANDESCENT LIGHT EMITTING DEVICES[*]

2.1. Introduction and Motivation

Modeling study of novel SSI-LED devices can be pivotal for their incorporation in future optoelectronic applications. An extensive literature review, as discussed in Section 1, shows that past studies done on SSI-LED have been mostly experimental in nature, and were more focused towards understanding the electrical and optical properties of this novel device.

In this section, the authors make use of computational techniques based on the well-known Finite Element Analysis (FEA) to perform electrothermal studies. A three-dimensional multi-physics model is set up to obtain stationary solutions using AC/DC and Heat Transfer modules in COMSOL Multiphysics® 5.2a software package. COMSOL Multiphysics is capable of combining electric currents and heat transfer into one model to study joule heating effects via coupled simulations. See Appendix A for basic steps to set up COMSOL simulation models. The ability to predict the local temperature distributions

_____

[*] Reprinted with permission from "Simulation of Electrothermal Characteristics of SSI-LED", by Abhinav Shukla and Yue Kuo, 2020. *ECS Trans.*, **97** (2), 69-77, Copyright 2020 by the Electrochemical Society.
[*] Reprinted with permission from "Study of Electrothermal Characteristics and Emitted Light Characteristics of SSI-LED," by Abhinav Shukla and Yue Kuo, 2020. *ECS J. Solid State Sci. Technol.*, **9** (6), 065017, Copyright 2020 by the authors, Open access.

in the nano-resistor and its vicinity at sub-nanometer scales through coupled electro- and thermal-effects is crucial in understanding the light emission phenomenon and elucidating the device's thermal behavior. The results obtained are correlated and utilized to explain reported physical observations on the device.

2.2. Model Description

2.2.1. Model Geometry

Conductive paths in Figure 5(a) are randomly and uniformly formed under the ITO electrode.[21] Hence, the distribution of nano-resistors is assumed to be random and is generated across the gate electrode area in the dielectric layer.

(a)   (b)
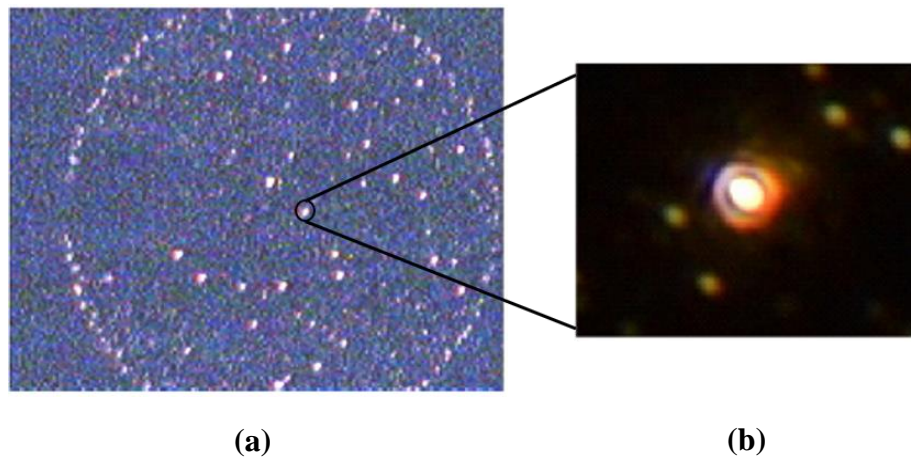
Figure 5. (a) High magnification photo of an SSI-LED with light emitted from nano-resistors[21], (b) light emitted from a single nano-resistor.[40]

Figure 6 presents the geometry of the model in a three-dimensional coordinate system. Typically, a silicon wafer has a thickness of 500 μm and diameter of up to 12 inches. Moreover, the reported number of conductive paths formed due to dielectric breakdown is quite high, e.g., in order of few thousands within a circle of 300 μm diameter.[27,35] However, in order to lower the computational complexity, the authors have considered representative device geometry with random distribution of about 50 nano-resistors of three different sizes – 20 nm, 50 nm and 100 nm. The size of the silicon substrate considered is 20 μm (length) × 20 μm (width) × 100 μm (thickness). The high-*k* dielectric film is taken to be HfO_2 of 10 nm thickness on top of a silicon wafer without considering a separate interface layer in the simulation. The ITO layer with thickness of 80 nm and diameter of 10 μm forms the gate electrode.
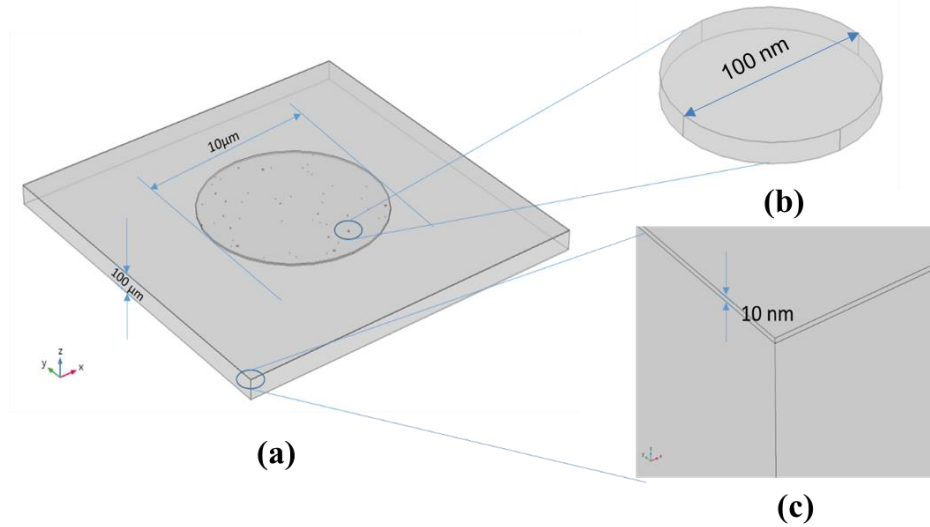
Figure 6. (a) The geometry of the SSI-LED in the COMSOL model with 80 nm thick ITO gate electrode. (b) A cylindrical nano-resistor of diameter 100 nm embedded in dielectric layer. (c) A thin high-k dielectric film (HfO$_2$) of thickness 10 nm.

2.2.2. Description of Governing Equations

The previous studies demonstrated that the leakage current density vs. gate voltage (J-V_g) curve of the SSI-LED at the $|V_g|$ larger than the breakdown voltage follows the Ohm's Law.[21] Hence, it can be assumed that the conductive paths formed in the dielectric behave as typical resistors. When stressed under the large V_g, nano-resistors experience Joule heating, which is a multi-physics process where the energy of an electric current is converted into heat as it flows through a resistor. A set of governing equations, as discussed below, were used to solve for the electric current density (J), heat flux density (q), potential distribution (V), and temperature distribution (T). The physics interface in

COMSOL solves a current conservation equation based on Ohm's Law using the scalar electric potential as the dependent variable. In a stationary coordinate system, the point form of Ohm's Law states that:

$$\boldsymbol{J} = \sigma\boldsymbol{E} \qquad\qquad [2.1]$$

where σ [S/m] is the electrical conductivity and $\boldsymbol{E}$ is the electric field strength. The static form of the equation of continuity then states:

$$\nabla \cdot \boldsymbol{J} = -\nabla \cdot (\sigma\nabla V) = 0 \qquad\qquad [2.2]$$

Similarly, the heat transfer process is modelled using the differential form of the heat equation (Fourier's Law) that may contain additional contributions like heat sources:

$$\rho C_p(\partial T/\partial t) + \rho C_p \boldsymbol{u} \cdot \nabla T + \nabla \cdot \boldsymbol{q} = Q \qquad\qquad [2.3]$$

$$\boldsymbol{q} = -k\nabla T \qquad\qquad [2.4]$$

where T [K] is temperature, q [J/m^{2}s] is heat flux, ρ [kg/m^3] is the solid density, C_p [J/K] is the solid heat capacity at constant pressure, k [W/mK] is the solid thermal conductivity, $\boldsymbol{u}$ is the velocity field when parts of the model are moving in material frame. In Equation 2.3, the first term on left hand side is the heat accumulation in any domain with time, the second term is the heat accumulation due to material flow, the third term is the heat transferred through that particular domain to the surrounding media, and Q on the right hand side accounts for heat generation in that domain. For a steady-state problem with no material flow, the temperature does not change with time and the first and second terms

17

in Eq. 2.3 disappear. For the nano-resistor domain, the Joule heating is accounted by utilizing the Multiphysics coupling feature in COMSOL, which adds the resistive heating as a heat generation source, Q, in the heat Eq. 2.3, and material properties may depend on temperature.

$$Q \ = \ \boldsymbol{J} \cdot \boldsymbol{E} \tag{2.5}$$

The electromagnetic surface losses are mapped as a heat source on the boundary in the heat transfer part of the model.

2.2.3. Boundary Conditions

Faces other than gate electrode and bottom of the silicon substrate were set to have an electric insulation boundary condition:

$$\boldsymbol{n} \cdot \boldsymbol{J} \ = \ \boldsymbol{0} \tag{2.6}$$

where $\boldsymbol{n}$ is the unit normal vector to the face. The electric potential of the silicon substrate's bottom is set to be 0 V, and all other potentials were measured with this reference. The top of the ITO layer (gate electrode) is set at the desired constant gate voltage, which is higher than the breakdown voltage reported experimentally (5). The Schottky barrier height at the nano-resistor to Si substrate contact, which was about 0.66 V[41], is insignificant compared to large gate voltage and, therefore, was neglected for model simplification. The thermal boundary conditions at the ITO gate/nano-resistor interface are modified based on the comparison between the experimental emission spectrum from a 300 μm diameter SSI-LED device with the black body radiation spectrum calculated from Planck's equation., as shown in Figure 7. Earlier studies suggesting that the color-

correlated temperature (CCT) of the SSI-LED lies typically between 2,500 K and 4,500 K acting as the reference to make an initial guess for the temperatures used in Planck's equation.[25] For instance, the peak of the spectrum recorded from an SSI-LED device closely matches with the radiation spectrum emitted from nano-resistors heated to 4,000 K, as inferred from Fig. 7. Hence, temperature distributions for cases with and without the nano-resistor/ITO interface set at 4,000 K are discussed.
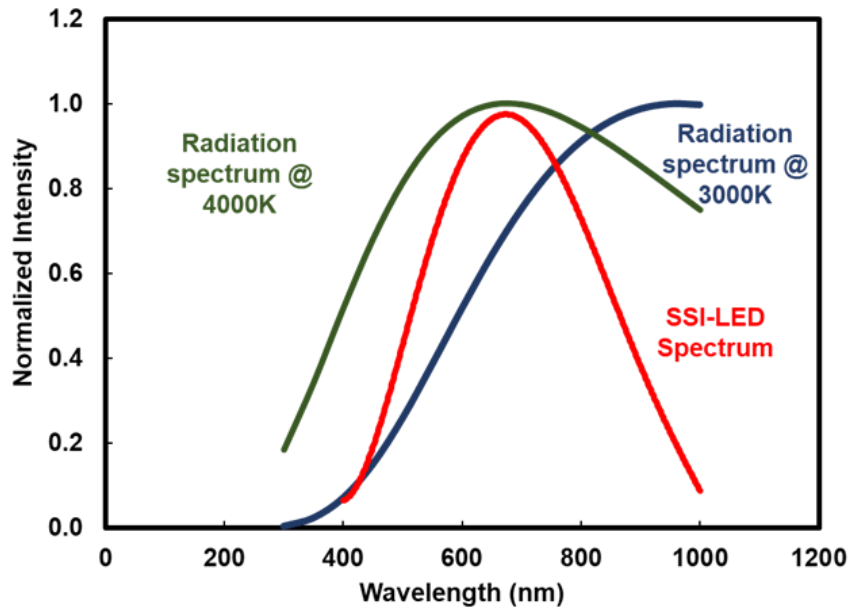
Figure 7. Black body emission spectrum at 3000 K and 4000 K respectively compared with SSI-LED emission spectrum when driven at -20V.

It is explicitly assumed that the temperature boundary condition of 4,000 K is applicable to nano-resistors of all sizes. This assumption is further proved through simplified energy balance-based calculations later in Section 5. Adiabatic boundary conditions are used at all the outer surface boundaries except at the top surface of the ITO gate and the bottom surface of the silicon substrate, i.e.,

$$\boldsymbol{n}.\boldsymbol{q} = 0 \qquad [2.7]$$

Two extremum boundary condition cases are discussed with respect to the top surface of the ITO gate:

Case I: Radiation and natural convection are considered at the top surface of the gate electrode at the ambient temperature (T_{amb}) of 300 K (assuming surface emissivity to be 0.11 for ITO):

$$\text{radiation: } \boldsymbol{n} \cdot \boldsymbol{q} = \eta\varepsilon(T_{amb}^4 - T^4) \qquad [2.8]$$

$$\text{natural convection: } q = h_{air}(T_{amb} - T) \qquad [2.9]$$

where $\eta = 5.6703 \times 10\text{-}8$ (W/m^{2}K^4) is the Stefan-Boltzmann Constant, ε is the surface emissivity of ITO taken to be 0.11 and, h_{air} is the convective heat transfer coefficient for air whose value depends upon the ITO gate dimensions, ambient pressure and temperature. The ambient pressure and temperature are taken to be 1 atm and 300 K respectively. Convective correlation developed for common geometries available in COMSOL are used to estimate heat transfer coefficients. In this model, vertical thin cylinder geometry corresponding to ITO gate is considered to estimate $h_{air.}$

Case II: A heat sink at temperature 300 K is added to the top gate surface, i.e., the temperature at the surface of the ITO electrode is fixed at 300 K.

Additionally, a temperature boundary condition of 300 K was applied to the bottom of the substrate and is common to both cases I and II. Material properties of the high-*k* dielectric film, substrate, and ITO gate, such as density, electrical conductivity, specific heat, thermal conductivity, and permittivity, were taken from literature[42-44] and are summarized in Table 1.

Table 1. Material properties of materials in different domains.

Domain	Material	Electrical Conductivity	Thermal Conductivity	Heat Capacity	Density
Substrate	p-type Si	7.4 [S/m]	130 [W/(m*K)]	700 [J/(kg*K)]	2329 [kg/m^3]
Dielectric	HfO$_2$	1E-9 [S/m]	1.06 [W/(m*K)]	120 [J/(kg*K)]	10330 [kg/m^3]
Gate Electrode	ITO	1E6 [S/m]	5 [W/(m*K)]	362.35 [J/(kg*K)]	7120 [kg/m^3]

Temperature independent electrical and thermal conductivities were used for calculations, except for those of nano-resistors. Since the material behavior of the nano-resistors is unknown, certain properties were estimated within the framework of scientific principles. For instance, the thermal conductivity was estimated using the Wiedemann-Franz Law, shown in Equation 2.10, which states that the ratio of the electronic contribution of the thermal conductivity (κ) to the electrical conductivity (σ) of a metal is proportional to the temperature:

$$\frac{k}{\sigma} = LT \hspace{4cm} [2.10]$$

where the proportionality constant L, known as the Lorenz Number, is equal to 2.44×10^{-8} W Ω K^{-2}. Electrical conductivity of conductive paths was calculated from the J-V_g characteristics of the SSI-LED device, as reported by Zhang et al.[35] The resistivity of the single nano-resistor was about 499 Ω·cm, 551 Ω·cm, and 601 Ω·cm for the -20, -30, and -40V stressed samples, respectively.[35] The increase in resistivity is attributed to increase in number of small nano-resistors formed in the dielectric. However, for the model simplification, the authors assumed that the number of nano-resistors were constant and independent of the increase of the gate voltage. The density and specific heat capacity of the nano-resistors were assumed to be the same as those of the hafnium oxide high-k dielectric material.[43,44]

2.2.4. Meshing Strategy in COMSOL

Creating a mesh in COMSOL comprises various steps and choices. The easiest way to resolve any geometry in COMSOL is by using the default Physics-controlled mesh, which is a simple, unstructured tetrahedral mesh. This default type mesh is automatically created and adapted for the model's physics settings. While this mesh does resolve the geometry well, it follows a uniform scheme throughout all domains of the geometry, even where fewer elements would be adequate, thus reducing memory requirements. In order to reduce mesh elements, the authors can manipulate the mesh to be finer at the circular (cylindrical in 3D) domains, representing the nano-resistors and the thin dielectric layer, and coarser throughout the rest of the geometry. The meshing scheme in this study

discretized the domains into triangular prism elements generated by sweeping triangular surface meshes across the z-direction with denser distribution in dielectric layer, as shown in Figure 8(b). The swept mesh scheme is adopted due to the geometry's high aspect ratio. It notably reduces the size of a model and its computational complexity. The triangular surface mesh was designed using a customized computational meshing sequence for different domains with a maximum element size of 2 μm, and a minimum element size of 0.008 μm. The mesh elements considered were still coarser in smaller domains due to limited computational resources.
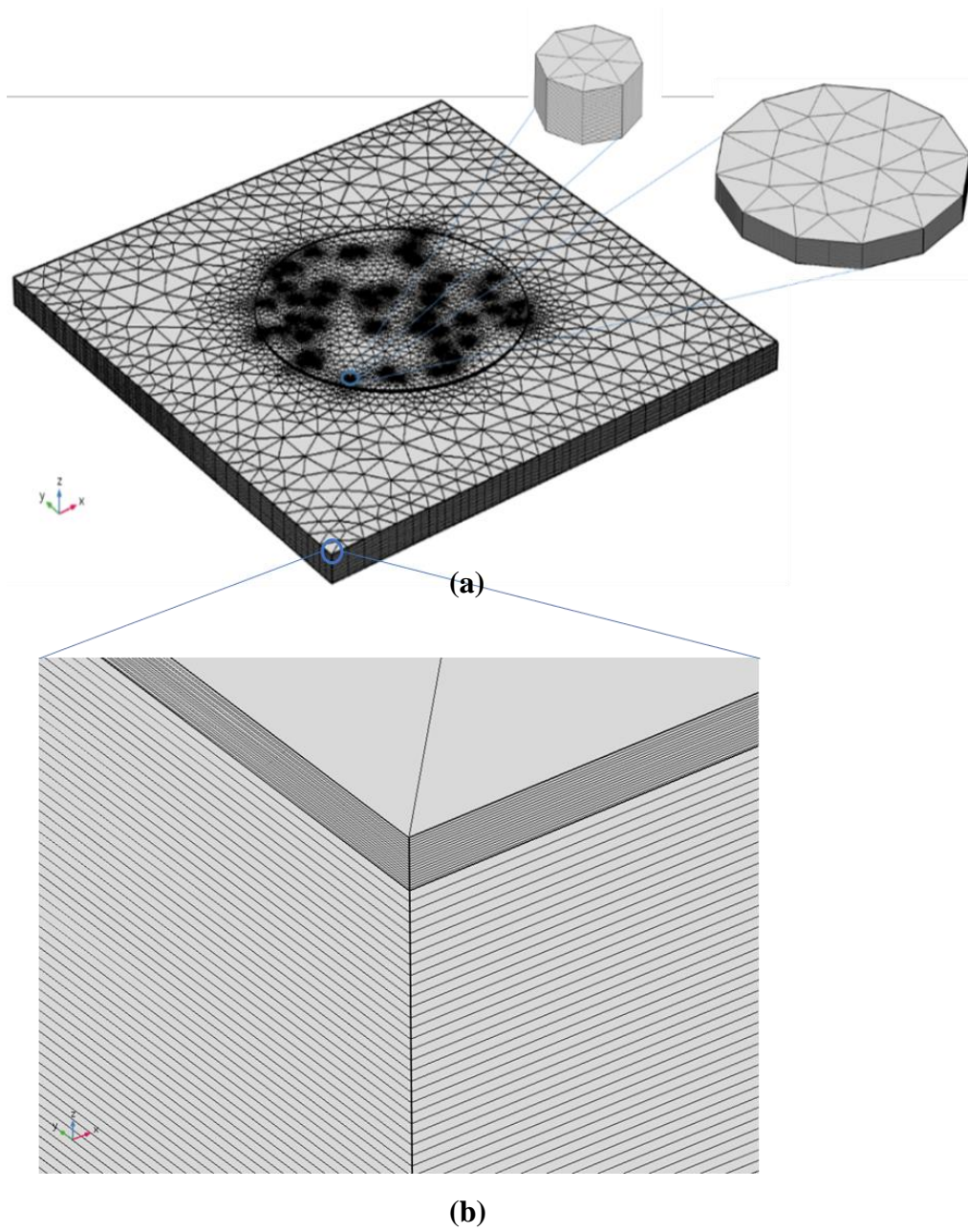
Figure 8. (a) Customized Model mesh for the solid state device defined in model geometry section with smaller mesh elements for nano-resistors, (b) Swept mesh in z-direction with denser distribution in dielectric layer.

24

2.3. Temperature Distribution Studies

The temperature distributions obtained in the nano-resistors, of diameters of 50 nm and 100 nm, and in the surrounding media at V_g = -20 V for Case I with no modified boundary conditions at the nano-resistor/ITO gate interface are shown in Figure 9(a) and 9(b), respectively. The simulation results discussed are for an actual SSI-LED device whose electrical properties were calculated at recorded current density of $J = 2 \times 10^2$ A/cm^2 when stressed at V_g = -20V.[21,35]
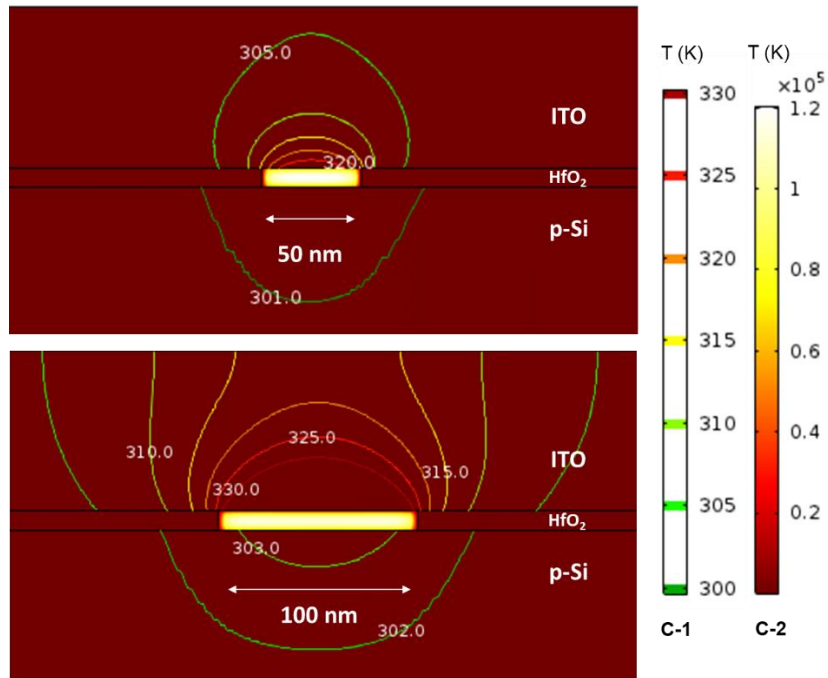
Figure 9. Simulated temperature (K) distribution obtained in the nano-resistors, of diameters (a) 50 nm, and (b) 100 nm, and in the surrounding media at V_g = -20V for Case I with no modified boundary conditions at nano-resistor/ITO gate interface. In this figure, the color scale C-1 corresponds to ITO and p-Si layer, and color bar C-2 is for nano-resistor domain.

The temperatures near the nano-resistor/ITO gate interface were close to 350 K, whereas temperatures near the nano-resistor/substrate interface were about 310 K. However, temperatures in the nano-resistor region were very high and in the order of magnitude of 5. Such high temperatures can be attributed to the large current passing through the few nano-resistors assumed to be distributed across the gate dielectric uniformly, and may be scaled down by accounting the actual number of nano-resistors formed, which is in the order of a few thousands within a circle of 300 μm diameter. The low temperatures recorded near the nano-resistor/ITO gate interface could not explain the earlier studies done by Lin et al. and Zhang et al.,[27,35] which showed the formation of many tiny bumps evenly distributed on the gate electrode surface. These bumps are claimed to be formed as a result of local melting of the ITO film and the underneath material, below which the nano-resistors had a very high temperature as suggested earlier.[41] Figure 10(a) shows a horizontal cross-sectional view of temperature distributions just below the nano-resistor/ITO interface of a nano-resistor in a SSI-LED driven at V_g = -20V. Nano-resistors of 3 different diameters are shown in this figure. The temperature in nano-resistor with diameter 20 nm and 50 nm decreases in radially outward direction. However, for large nano-resistors of diameter 100 nm, temperature initially decreases radially but spikes again close to the edge and eventually drops at edge. This sudden increase of temperature near the nano-resistor's edge can be attributed to the large current density near the edge caused by charge carrier accumulation because of large difference in electrical conductivities in the bulk nano-resistor and at the nano-resistor/surrounding dielectric

26

interface. Figure 10(b) shows the vertical cross-sectional views of current density distributions obtained in and around nano-resistors of size 50 nm and 100 nm, respectively. Such sudden increase in temperatures along the radial direction is not seen in smaller nano-resistors as there is no significant radial variation in current density.
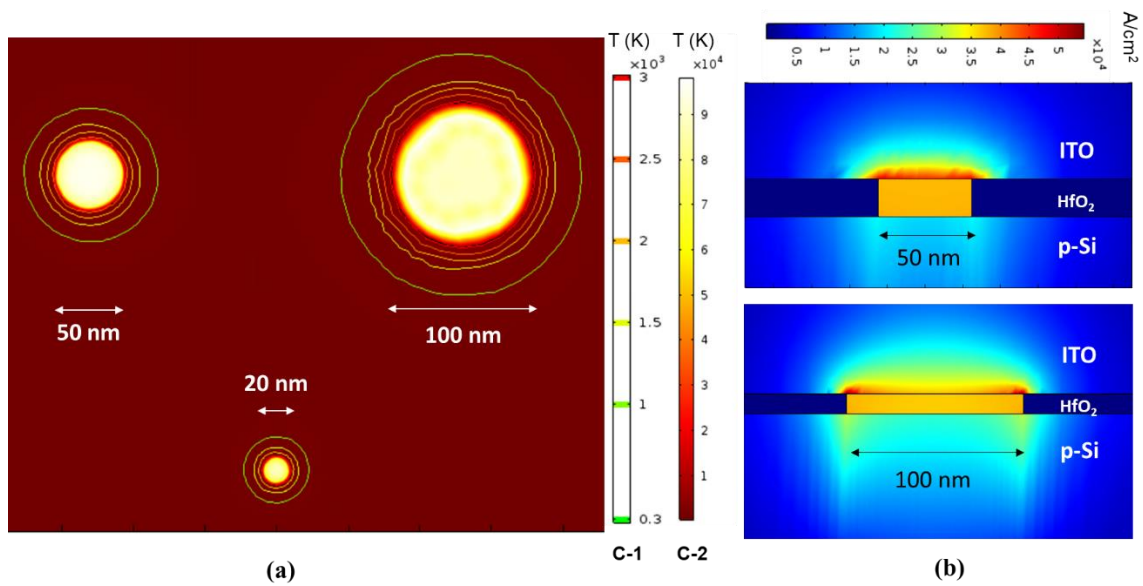
Figure 10. (a) Horizontal cross-sectional view of simulated temperature (K) distribution in nano-resistors of 3 different diameters vertical to current flow direction. In this figure, the color scale C-1 is for dielectric domain whereas color bar C-2 is for nano-resistor domain. (b) Vertical cross-sectional view parallel to current flow direction of current density (A/cm^2) in nano-resistors of diameter 50 nm and 100 nm, respectively.

Temperature distributions with modified boundary conditions at nano-resistor/ITO interface obtained in the nano-resistors of diameters of 50 nm and 100 nm and in the surrounding media under boundary condition cases I and II are shown in Figure 11(a) and 11(b), respectively. Maximum temperatures in the region close to nano-resistor/ITO interface were higher than the melting temperature range of the ITO, i.e., 1800-2200 K in
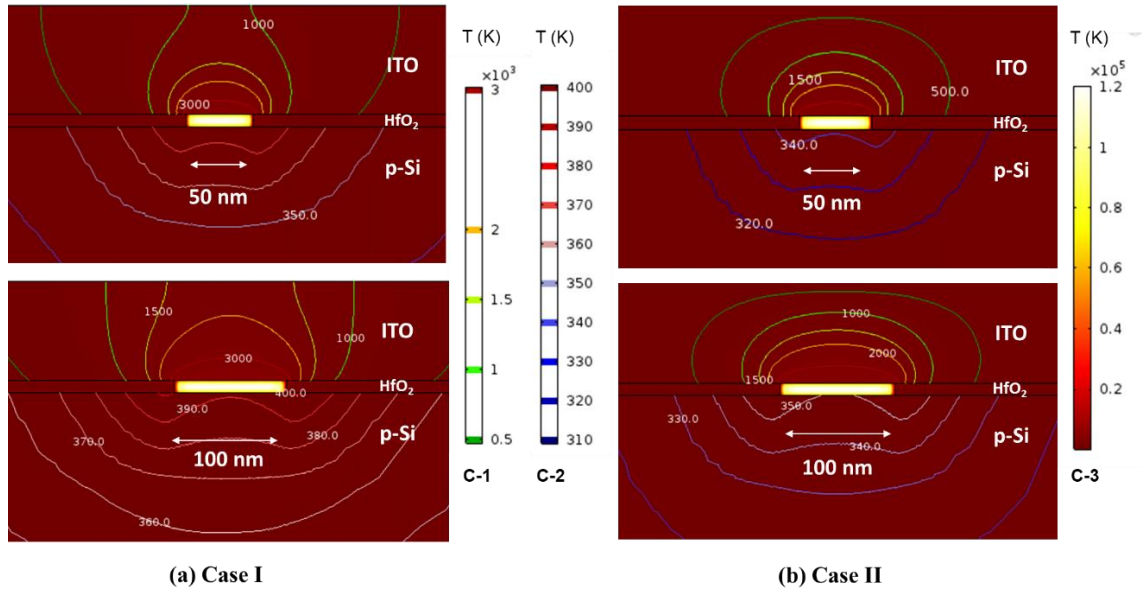
(a) Case I   (b) Case II

Figure 11. Vertical cross-sectional view of temperature (K) distributions in and outside of 50 and 100 nm diameter nano-resistors at Vg = -20V for (a) Case I and (b) Case II with modified boundary condition at nano-resistor/ITO interface. The left color scale (C-1) is for ITO layer, middle color scale (C-2) is for p-Si domain and rightmost color bar (C-3) is for nano-resistor domain. The color scales and color bar shown are common to Fig. 11(a) and 11(b).

both cases. This result supports previous studies[27,35] that the bumps located above nano-resistors are formed because of local melting of ITO. Intense heating occurs in the nano-resistors due to the passage of the large current. The heat generated is carried away through the gate electrode layer and the substrate. It is possible to see the effect of increasing gate voltage on the spread of heat in the region close to nano-resistors. The spread in the substrate is not as significant as that in the gate due to silicon's high thermal conductivity (~130 W/m-K), which results in better heat transport and removal.

2.4. Summary

In summary, temperature distributions in the SSI-LED device, especially inside nano-resistors and in the regions surrounding nano-resistors, were obtained with optimized boundary conditions based on correlative studies between blackbody radiation and optical emission spectrum. The high temperatures recorded near the nano-resistor/ITO gate interface confirmed that the experimentally observed bumps formed over the ITO gate electrode as a result of localized melting. This melting is caused by extreme heating due to passage of large currents through the nano-resistors. The gate voltage is found to affect the distribution of heat in the vicinity of the nano-resistor, i.e., in the dielectric, gate electrode and silicon substrate. The current density variation near the edge of the large nano-resistors affected the local temperature distribution across the cross-section of nano-resistors.

Moreover, it can be stated from the thermal analysis of the solid state device that the domain of heat generation in the device is confined to very small regions. These

29

regions are on the order of the phonon mean free path. Conventional Fourier analysis, as utilized in COMSOL, may not be enough to explain the physics of heat transfer happening in regions with smaller length scales. This is due to the assumption that heat transport occurs diffusively at infinite wave speed, i.e., molecule-molecule collisions are predominant. However, this is not true as transport becomes ballistic in nature at smaller length scales and heat is transferred by phononic interactions.[45] Improved temperature estimation may require a solution of the appropriate phonon transport equations.

3. COMPARISON OF SIMULATED AND MEASURED LIGHT EMISSION SPECTRA FROM SOLID STATE INCANDESCENT LIGHT EMITTING DEVICES[*]

3.1. Introduction and Motivation

Besides the light emission applications, the novel behavior of nano-resistors based SSI-LEDs allows it to be potentially integrated in many different fields.[24,46] As discussed in review of SSI-LED in Section 1, the emitted light can be narrowed down using thin film filters like hydrogenated amorphous silicon (a-Si:H), making such devices a potential Si-based light source for on-chip optical interconnect systems.[37] Optical interconnection can be the ultimate solution to the signal delay in ultra-high-density ICs.[47] It has been reported that light source with narrow bandwidth is desirable for the on-chip optical interconnect in order to achieve a high contrast ratio between on and off states.[48,49] Zhang and Kuo showed that when the SSI-LED was coated with an a-Si film, the spectrum of the emitted light was shifted from the range of 450 nm-950 nm to the range of 530 nm-950 nm and the peak was moved from 700 nm to 810 nm.[37] Moreover, the emission spectrum can be transformed into a major narrow peak at 850 nm with a bandwidth of ~8 nm and a minor peak of 650 nm using a 9-layer $(HL)^2HH(LH)^2$ Fabry-Perot filter where H and L are 52.0 nm thick a-Si:H film and 105.9 nm thick SiN_x film, respectively.[37]

Additionally, Shukla and Kuo recently reported that the equivalent blackbody temperature of nano-resistors, formed in the high-*k* dielectric thin film, responsible for the light emission is around 4,000 K.[50] Therefore, in this section, the authors model the light emission spectrum from the SSI-LED and theoretically investigate the effect of thin film filters. The emission spectra from the thermal excitation of the nano-resistor at different temperatures with and without inclusion of an ITO or a-Si thin film filter are computed and compared with those measured from actual devices.

3.2. Methodology and Comparative Studies of Emission Spectra

Spectral radiance B(λ,T), which is the power emitted per unit area of the body, per unit solid angle of emission in the wavelength interval λ to λ + Δλ (Δλ denotes an increment of wavelength) at absolute temperature T, from the black-body radiation theory according to the Planck's Law,[51,52] is utilized to calculate theoretical emission spectrum using equation 4.1:

$$B(\lambda, T) \; = \; \frac{2hc^2}{\exp\left(\frac{hc}{kT\lambda}\right)-1} \qquad\qquad [3.1]$$

where h is Planck's constant, c is the speed of light and k is the Boltzmann constant. The calculated spectra are all normalized for comparison purposes. Note that in this study it is assumed that under the same gate voltage driven condition, the temperature of the nano-resistor does not vary with size.

As discussed in Section 2, Fig. 7 shows that the peak of the spectrum recorded from an SSI-LED device closely matches with the radiation spectrum emitted from nano-resistors heated to 4,000 K. This is consistent with the earlier studies suggesting that the color-correlated temperature (CCT) of the SSI-LED lies typically between 2,500 K and 4,500 K, which is a function of gate voltage, dielectric material, and processing parameters.[25] Additionally, electrothermal calculations under certain assumptions have been performed earlier to estimate temperatures in and around the conductive paths formed in the gate dielectric.[50] Hence, radiation spectrum of a blackbody at 4,000 K is exploited for the further study on the effect of the thin film filter on the emission spectra calculated theoretically from the Planck equation and light absorption data, which is measured experimentally. See MATLAB script in Appendix C for details on theoretical calculations.

3.2.1.1. ITO thin film filter

Note that the SSI-LED spectrum in Fig. 7 was recorded from the device with an ITO gate. Figure 12 shows the comparison of spectrum of the black body emission at 4,000 K filtered with an annealed ITO film and that measured from a SSI-LED made from ref. 22 process. The experimental optical transmittance data of a 500 nm thick annealed ITO film was taken from the literature.[53] Although the ITO layer thickness in the SSI-LED was only 80 nm, the result on the ITO filtration effect does not change based on the assumption that the thickness only changes the light intensity not the spectral distribution.
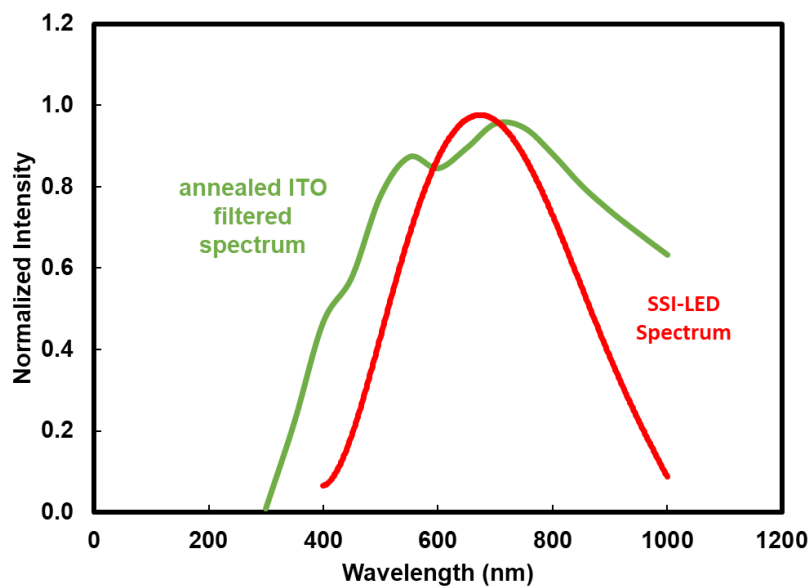
Figure 12. Comparison between blackbody radiation spectrum filtered by an ITO thin film and an SSI-LED (with ITO gate) emission spectrum.

The filtered blackbody radiation spectrum shows a major peak near 750 nm in addition to a satellite peak near 550 nm. The major peak is observed to be close to the peak wavelength of SSI-LED emission spectrum. The slight deviation of major peak towards left of experimental spectrum might be due to the fact that ITO melts when the device is in operation as suggested by Zhang et al.[35] and corroborated by Shukla et. al.[50] The determination of optical transmittance of molten ITO over the visible and IR wavelengths might help in achieving more precise comparisons.

3.2.2. a-Si:H thin film filter

Similar calculations were made for a-Si:H thin film filters. The optical transmittance data was calculated using spectral dependence of optical absorption coefficient for a CVD a-Si thin film as reported by Hirose et. al.[54] The data reported corresponds to thin films with thickness in range of 0.5 - 1 μm. However, in our calculations, the transmittance of the a-Si film was estimated from that of a 100 nm thick film adjusted with the Beer-Lambert's Law. Figure 13 shows the comparison between experimental spectrum recorded from an SSI-LED with a-Si thin film filter (blue curve) of thickness 100 nm deposited using PECVD process as discussed in ref. 37, and theoretically calculated spectrum (red curve) obtained from blackbody radiation at 4,000 K filtered with a-Si:H thin film of thickness 100 nm.

For the a-Si:H filter, the light below the 450 nm wavelength disappears. This observation of absorption in short wavelength range is consistent with the earlier literature reports.[54-56] The peak of the theoretical spectrum with a-Si thin film filter was found to be off towards the long wavelength range compared to the experimentally recorded spectrum. This deviation may be attributed to the fact that the a-Si thin film melts from the intense heat conducted from underneath nano-resistors.[50] It is highly likely that the a-Si film over the nano-resistors recrystallizes and forms poly-Si at such high temperatures. Therefore, we extended our study to see the effect of the poly-Si thin film filter on the blackbody radiation spectrum of the nano-resistors. The optical transmittance data for poly-Si thin film was calculated in a similar way as that of a-Si thin film based on the absorption coefficient data reported in ref. 54. The absorption coefficient data used corresponds to
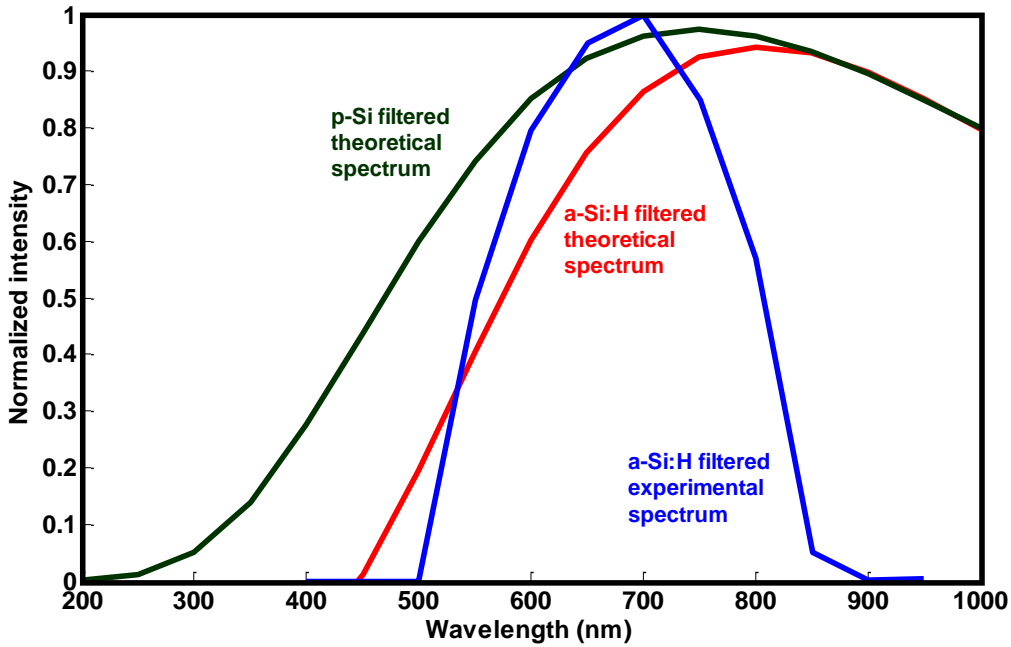
Figure 13. Comparison between theoretically calculated and experimentally measured emission spectrum (blue) for an SSI-LED with a-Si (red) and poly-Si (green) thin film filter.

that of a poly-Si thin film prepared by the annealing of as-grown a-Si film in nitrogen gas for 1 hour in the temperature range of 700-1050°C.[54] The green curve in Fig. 13 shows the comparison of emission spectra of 100nm-thick poly-Si filtered SSI-LEDs, calculated from the blackbody radiation equation assuming nano-resistors are heated to 4,000 K, to that measured from the actual device.

The wavelength corresponding to peak of the computed spectrum for the poly-Si thin film filtered device is found to be in closer proximity to that of the actual device than that of a-Si thin film filtered device shown in Fig. 13. Although, this suggests that a-Si

may have recrystallized under the device's light emission condition, it might be possible that it stays in the molten state during device operation, like in the ITO filter case as discussed previously. More studies will be carried out when the optical transmittance of the molten silicon phase over visible wavelength range is available. In the higher wavelength range, the theoretical and experimental emission spectra for both a-Si and poly-Si filters are not observed to be in good agreement. Note that Si filters studied here are formed over the SSI-LED with the ITO gate electrode. Previous reports on compositional analysis of the high-k stack with the ITO gate electrode in SSI-LED show significant amount of Si in the ITO layer.[27] Therefore, it is probable that, in SSI-LEDs with a top silicon filter, silicon atoms can diffuse from the bulk Si wafer through nano-resistors into the ITO layer which results in variation in emitted light characteristics. Although, there have been very few studies on optical properties of Si doped ITO filters, it is reported that films prepared by co-sputtering ITO and SiO_2 at higher power ratios (ITO/SiO_2) have high extinction coefficients at longer wavelengths in the visible range when compared to that of films deposited at low power ratios.[57] This suggests that presence of Si in ITO may decrease the transmittance for longer wavelengths in visible range which is consistent with the experimental emission spectra in Fig. 13.
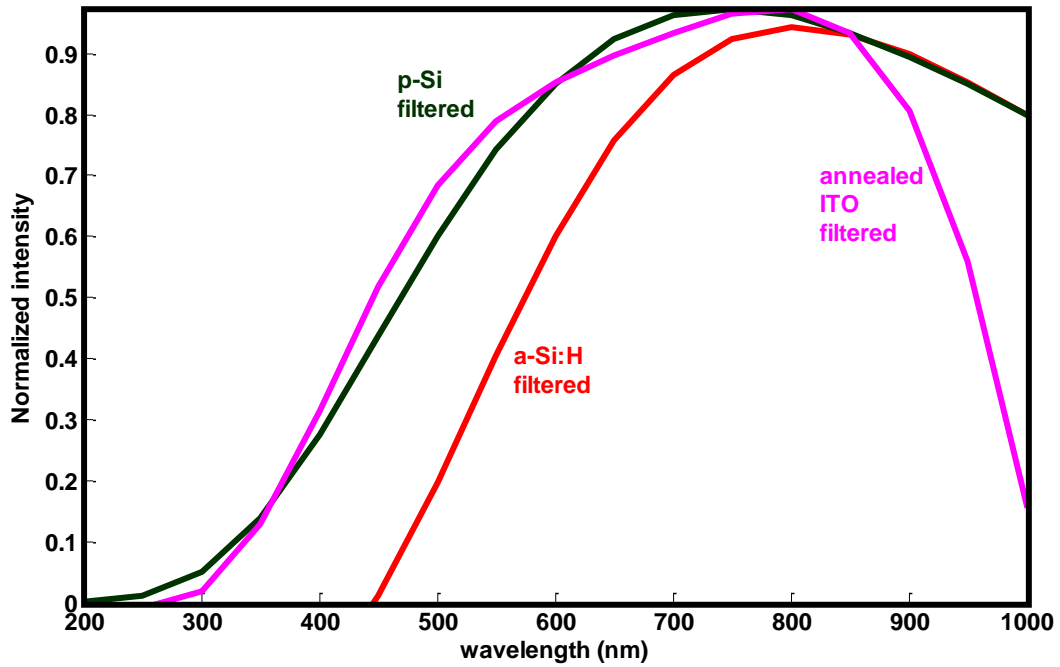
Figure 14. Comparison of theoretically calculated emission spectrum for SSI-LED with a-Si:H (red), poly-Si (green) and ITO (pink) thin film filters respectively.

Figure 14 shows the comparison of theoretically calculated emission spectrum for SSI-LED with a-Si:H, poly-Si and ITO thin film filters of thickness 100 nm respectively. The shorter wavelength range, below 500 nm, has appreciable transmittivity through poly-Si and ITO thin film filters as compared to a-Si:H thin film with almost negligible transmission. The peak wavelengths corresponding to poly-Si and ITO filtered spectrum are nearly same and lie close to 750 nm. However, the peak wavelength for a-Si filtered spectrum lies between 800-850 nm. In the long wavelength range, the transmittivities of

38

a-Si:H and poly-Si are almost the same as well as quite significant as compared to that of decreasing transmittivity of ITO thin film filter.
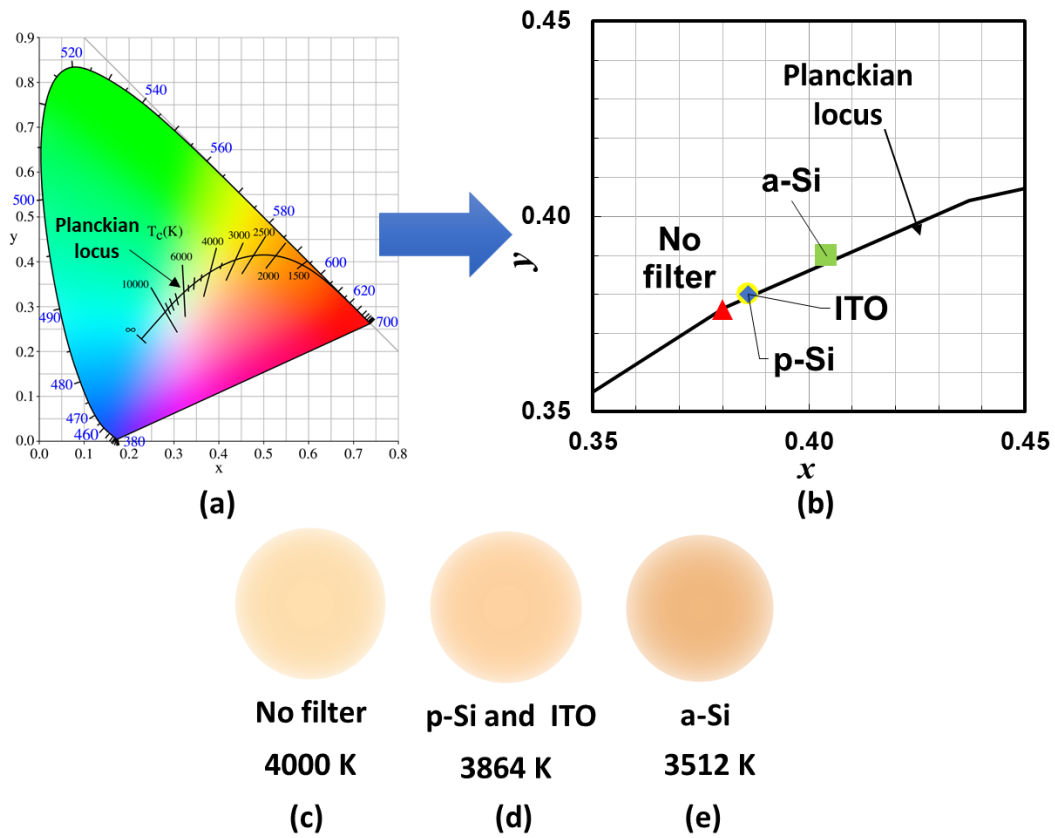
Figure 15. (a) CIE 1931 chart, (b) enlarged view of (a) with x-y chromaticity co-ordinates of light dots corresponding to nano-resistors with (c) no filter, (d) ITO or poly-Si filter, and (e) a-Si filter.

Calculated emission spectra for SSI-LEDs with different thin film filters can be utilized to find light characters such as color correlated temperatures (CCT's) and CIE chromaticity coordinates. The CCT can be calculated using peak wavelength (Wein's Displacement Law) of the theoretical emission spectrum for each type of thin film filter in Fig. 14. Additionally, the CIE 1931 color space, created by the International Commission on Illumination in 1931,[58] can describe all visible colors to the human eye. The CIE (x, y) chromaticity diagram shown in Figure 15(a) is widely used and is obtained from the spectral power distribution of the light source and the CIE color-matching functions.[59] See Appendix B for more details on CIE chromaticity co-ordinates calculations.

Table 2. Calculated peak wavelengths, corresponding CCTs and CIE (x,y) chromaticity coordinates of lights emitted from a nano-resistor without a filter and with a filter made of a-Si, poly-Si and ITO, respectively.

	λ_{peak} (nm)	CCT (Kelvins)	CIE (x,y)
No filter	724.4	4000 K	(0.380,0.376)
a-Si	825	3512 K	(0.404,0.390)
poly-Si	750	3864 K	(0.386, 0.380)
ITO	750	3864 K	(0.386, 0.380)

Table 2 summarizes the calculated peak wavelengths, corresponding CCT's and CIE (x,y) chromaticity coordinates for emission spectra from the same nano-resistor without a filter and with different filters. The color corresponding to each filtered spectrum is obtained from locating the CCT value on the Planckian locus. Fig. 15(c) is the light dot perceived from a nano-resistor heated at 4,000 K with no filter whereas Fig. 15(d) and (e) show light dots corresponding to the same nano-resistor filtered with poly-Si (or ITO) and a-Si thin films, separately. As shown in Fig. 15, lights emitted from the poly-Si and ITO filtered dots almost overlap in the visible wavelength range.

3.3. Summary

In this section, the light filtration effect of ITO and a-Si:H thin films on the broad-band light emitted from the ZrHfO high-k dielectric based SSI-LED has been theoretically investigated and compared with the experimental observations. The study suggested that the ITO thin film filter above nano-resistors formed in the dielectric film may melt due to intense Joule heating during the passage of a large current. Similar conclusions were made for the SSI-LED with a-Si thin film filter where the experimental spectrum more closely fitted with the computed spectrum corresponding to SSI-LED with poly-Si thin film filter. The deviation in experimental emission spectrum from simulated spectrum, for SSI-LEDs with a-Si and poly-Si thin film filters, for longer wavelengths in visible range is attributed to variation in optical properties of ITO caused by diffusion of silicon atoms at elevated temperatures. The a-Si film may recrystallize to form poly-Si during operating conditions. Further, simulated light emission spectra for SSI-LEDs with different thin film filters are

characterized using corresponding CCT's and CIE (x,y) chromaticity diagram. Emitted light characteristics of device with poly-Si and ITO filters are found to be similar in nature. In summary, the broadband light emitted from the SSI-LED can be narrowed down with the addition of thin film filters. The peak of the new spectrum is found to be dependent upon the optical properties of the material of the filter.

4. LIGHT INTENSITY DISTRIBUTION STUDIES IN SSI-LED[*]

4.1. Introduction and Motivation

In Section 3, the finite element-based simulation study of electro-thermal characteristics of the SSI-LED confirms that the intense heating is occurring inside the nano-resistors, which is causing light emission. Section 4 made use of Planck's Law of blackbody radiation to theoretically model the light emission spectrum from SSI-LED and presented comparative studies with actual SSI-LEDs, including effects of thin film filters. However, there is a lack of studies on SSI-LED's emitted light intensity distribution. In this section, the authors study the light intensity distribution from SSI-LED by treating nano-resistors as black body objects and the emitted energy as blackbody radiation. The light intensities at various vertical distances are investigated through computational calculations. Additionally, the effect of the nano-resistors' geometrical layout on local variation in light intensities is also discussed.

4.2. Model Setup and Parameters Estimation

In addition to the high CCT, SSI-LEDs are reported to have a high color rendering index (CRI) of up to 97.9, which is close to a perfect 100 of an incandescent light bulb.[27] This suggests that the light emission process from nano-resistors, heated to high temperatures

_____

in the SSI-LED, is similar to the black body radiation phenomenon. Therefore, to study

the emitted light intensity distribution from the SSI-LED, the authors assumed that nano-

resistors formed in the dielectric behave as ideal blackbody radiators and the total emitted

energy from each of these nano-sized radiators is treated as blackbody radiation. The well-

established Stefan-Boltzmann Law,[60,61] given in equation 5.1, states that the total energy

radiated per unit surface area of a blackbody object across all wavelengths per unit time,

j^*, is directly proportional to the fourth power of the black body's absolute temperature T,

i.e.,

$$j^* = e\sigma T^4 \qquad [4.1]$$

where e is the emissivity of the object ($e = 1$ for perfect black body) and σ is the Stefan–

Boltzmann constant. Hence, total power radiated from an object of surface area A can be

given by Equation 5.2,

$$P = Aj^* = Ae\sigma T^4 \qquad [4.2]$$

Moreover, if a black body is radiating energy to the surroundings at temperature T_c,

assumed to be 298 K, the net power radiated can be accounted as given in Equation 5.3,

$$P = Ae\sigma(T^4 - T_c^4) \qquad [4.3]$$

Further, the authors assumed that each of the nano-resistors emitting blackbody radiation

is a point source based on their very small dimensions compared to the gate diameter.

Therefore, the authors calculated the emitted radiation intensity at a given distance from

each of the nano-resistors by following inverse-square law according to which the

intensity, I, of radiation emitted from a point source varies inversely with the square of

the distance, r, from the source. Mathematically,

$$I = \frac{P}{4\pi r^2} \qquad [4.4]$$

So, the calculation of resultant intensity contributed from all the nano-resistors at any given point in space is straightforward and will be the scalar addition of radiation intensity from each individual light sources, i.e., if I_1, I_2...., I_N are the radiation intensities due to N nano-resistors at a point in space then the resultant intensity,

$$I_{resultant} = I_1 + I_2 + I_3 \ldots \ldots \ldots + I_N \qquad [4.5]$$

Certain assumptions, based on earlier studies reported on the SSI-LED, were made for various physical parameters while calculating the radiation intensity distribution from the SSI-LED. For instance, nano-resistors with circular cross-sections were assumed to form in the high-*k* dielectric for easier estimation of object surface area in Eq. 5.2. The nano-resistors were randomly distributed across the high-*k* gate stack based on the earlier studies suggesting that the hard breakdown process in ultrathin gate oxide is purely random, and the breakdown sites cannot be predetermined.[62] The nano-resistors are distributed such that the distance between any two adjacent nano-resistors is not less than 200 nm, which is twice the reported minimum distance between two consecutive weak spots in gate oxides.[63] To enhance the calculations' accuracy, the authors considered a size-based distribution of nano-resistors in the SSI-LED in accordance with the SEM characterizations that reported evenly distributed bumps, of varied sizes, formed over the ITO electrode surface.[35] 200, 500 and 1000 nano-resistors of diameters 20 nm, 50 nm, and 100 nm are randomly distributed across the gate dielectric of diameter 100 μm in the number ratio of 70%, 25%, and 5%. Shukla et al. report that the peak wavelengths in the emission spectrum recorded from an SSI-LED driven at the gate voltage V_g = -20 V

45

matches with the peak wavelength of the blackbody radiation spectrum from nano-resistors heated to 4,000 K.[50,64] Based on this and the assumption that nano-resistors behave as black body radiators, their absolute temperature is taken to be 4,000 K, irrespective of the size, and is utilized for calculating net radiated power in Eq. 5.3. The authors neglected size effect on temperature variation in nano-resistors based on the calculations that assume adiabatic condition. The adiabatic condition refers to the case when the entire joule heat generated in nano-resistors is used to raise the temperature of the nano-resistors with no heat loss to the surrounding media of the high-k dielectric, the Si wafer, or the ITO electrode. The adiabatic assumption is supported by the fact that there exists a significant difference between thermal conductivity coefficients of the gate dielectric surrounding the nano-resistor, e.g., 1.06 W/m-K for HfO_2[65] and a conductor, e.g., >5000 W/m-K for hafnium silicides,[66] in a SSI-LED. Therefore, the final temperature of nano-resistors can be estimated by performing simple energy balance, as shown in Equation 5.6,

$$I \times V \times \Delta t = m \times C_p \times \Delta T \hspace{2cm} [4.6]$$

where I is the current passing through a nano-resistor, V is applied gate voltage V_g, Δt is the time taken by nano-resistor to achieve final steady state temperature from initial room temperature of 298 K, m is the mass of the nano-resistor, C_p is the heat capacity of the nano-resistor at constant pressure, and ΔT is the temperature difference between final steady state temperature and initial room temperature. Resistivity of nano-resistor at $V_g = -20\,V$ is estimated to be about 499 Ω-cm.[35] Therefore, resistance of nano-resistors with different diameters can be estimated using Pouillet's Law, $R = \rho.L/A$, where R is the

46

resistance, ρ is the resistivity, L is the length, and A is the cross-sectional area. The estimated resistances for nano-resistors of diameter 20 nm, 50 nm and 100 nm are $1.592 \times 10^8 \Omega$, $2.546 \times 10^7 \Omega$ and $6.366 \times 10^6 \Omega$ respectively, assuming the length of the nano-resistor is same as the thickness of the high-k dielectric, i.e., 10 nm.[21] Hence, current through each of the nano-resistors at $V_g = -20\ V$ can be calculated following Ohm's Law. The time taken by the SSI-LED to achieve steady state conditions is estimated to be of the order of few nanoseconds and is taken to be about 13 ns in the above calculations.[25] Assuming the density and C_p of the nano-resistor to be same as that of HfO₂, i.e., 10,330 kg/m³ and 285.9 J/kg-K[42-44], the final steady state temperature is about 3,818 K in the nano-resistor of diameter 20 nm, and 3,820 K in nano-resistors of diameters 50 nm and 100 nm respectively. The estimated temperatures are quite close to 4,000 K, as considered before in Section 2, based on SSI-LED's emission spectrum. No significant variation in the temperature of nano-resistors with varying sizes can be attributed to the constant current to mass ratio in the nano-resistors.

Lastly, to account for the light absorption by the ITO thin film for intensity calculations, the authors make use of Beer-Lambert's Law. The optical absorption coefficients in ITO thin films, in the visible and some infrared wavelength range of 400 nm – 1,240 nm, are very low and almost constant[67]. The reported transmittance is about 89.1% for a film of thickness 200 nm for both annealed and unannealed films.[67] Therefore, the constant absorption coefficient in the visible range is back calculated from the available transmittance data, and then the absorption effect is adjusted for the ITO film of thickness 80 nm, as deposited in the SSI-LED. The authors initially perform emitted

radiation intensity distribution calculations from only two nano-resistor sources before discussing the detailed 3-dimensional (3D) results. All the calculations were performed using MATLAB on a Dell Optiplex workstation powered by Intel(R) Core (TM) i7-2600 CPU@3.40GHz running Windows 10 operating system. See MATLAB script in Appendix D for details on numerical calculations setup.

4.3. Light Intensity Distribution Studies

Figure 16 shows the light intensity distribution emitted from two adjacent nano-resistors, S1 and S2, each of 100 nm diameter, formed at different inter nano-resistor distances of 100 nm, 200 nm, and 500 nm. Each of the plots in Fig. 16 are obtained at increasing vertical distances from the nano-resistor/ITO interface. At smaller distances of 80 nm or less, two sharp intensity peaks can be observed for the inter nano-resistor distances of 200 nm and 500 nm. However, nano-resistors formed 100 nm apart are difficult to resolve even at small distances of 80 nm from the nano-resistor/ITO interface. At more considerable distances of 150 nm or higher, the peaks seem to merge, and at distances as large as 2 mm, which is typically the object distance at low magnification, the nano-resistors are completely unresolvable. This corroborates the experimental observation that discrete light sources in a SSI-LED can be detected by a high magnification microscope, but only a single light image can be observed with a low magnification microscope.[21]
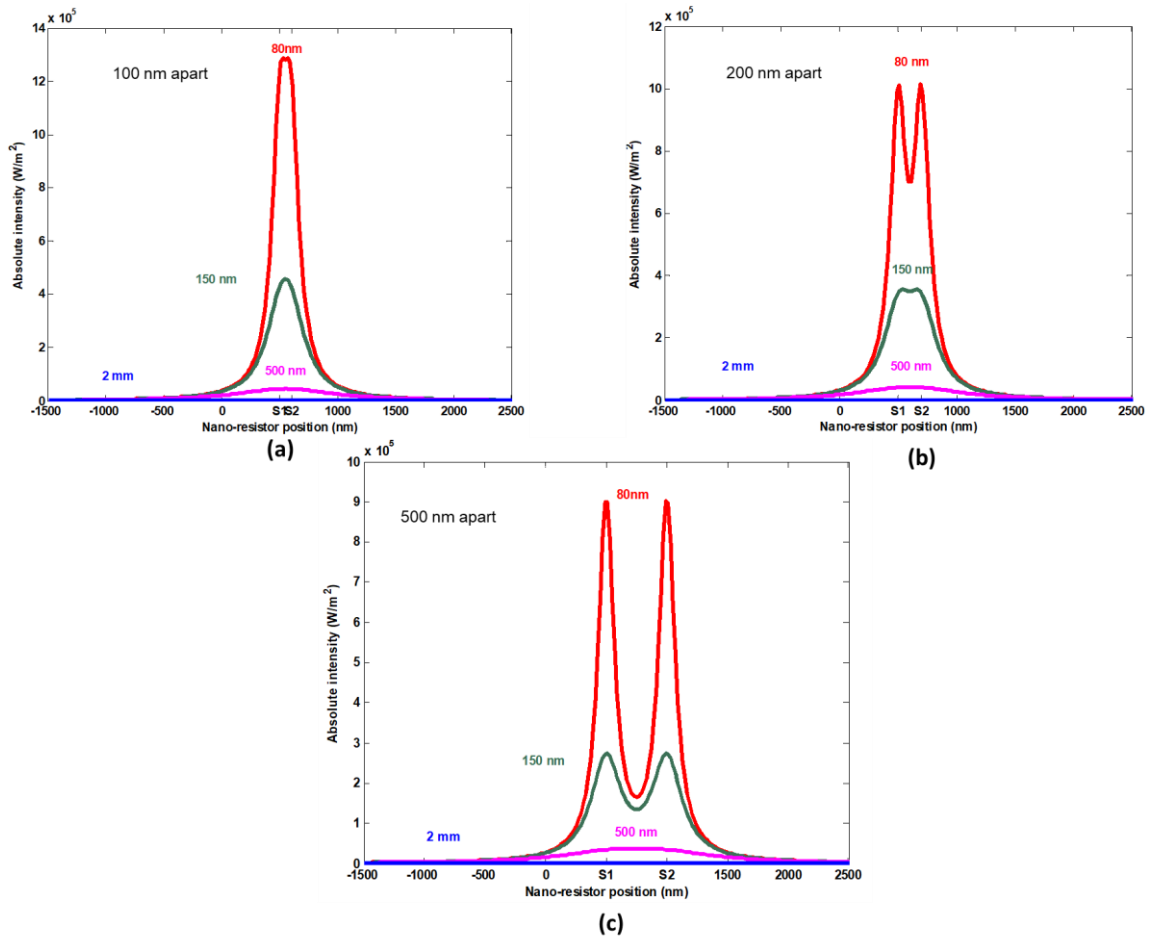
Figure 16 . Light intensity distribution emitted from two adjacent nano-resistors S1 and S2, each of 100 nm diameter, formed (a) 100 nm, (b) 200 nm and (c) 500 nm apart. Intensity variation plots in each figure are at increasing vertical distances from the nano-resistor/ITO interface.

Figure 17 shows the (a) top and (b) tilt views of emitted light intensity distribution from a SSI-LED of 100 μm diameter with 200 randomly distributed nano-resistors at a distance of 80 nm above the dielectric/ITO interface. The 200 nano-resistors constitute of 140 20 nm, 50 50 nm and 10 100 nm diameter sized nano-resistors. The larger bright red spots in

Fig. 17(a) and the corresponding intensity spikes in Fig. 17(b) are observed mainly due to cluster formation of nano-resistors in certain regions, increasing the intensity, which is the algebraic sum of intensity from all adjacent individual nano-resistors. Additionally, the intensity depends on the total power emanating from nano-resistors, which further varies directly with the cross-sectional surface area. Therefore, the observation of some of the large bright red spots can also be attributed to the increased light intensity from large sized nano-resistors formed in certain regions. The reported number of nano-resistors formed in the gate dielectric at larger gate voltages is higher than that at low gate voltages, and the SEM micrograph studies report a different size-based distribution from what is observed at lower gate voltages.[35] Figure 18 shows (a) top and (b) tilt views of emitted light distributions from a SSI-LED of 100 μm diameter with 1000 nano-resistors composed of 850 20 nm, 110 50 nm and 40 100 nm diameters based on the size distribution reported at V_g = -40 V (15). Both Fig. 17(a) and Fig. 18(a) show formation of large and small bright red spots, except that the number of larger bright red spots appear to increase significantly in the later. Moreover, a greater number of smaller bright red spots are also visible in Fig. 18(a) than that of in Fig. 17(a). This is expected as the number ratio of smaller sized nano-resistors is quite significant for the case when 1000 nano-resistors are considered, as compared to 200 nano-resistors. The increase in number of larger bright red spots may be due to the increase in nano-resistors clusters and the number of large sized nano-resistors.
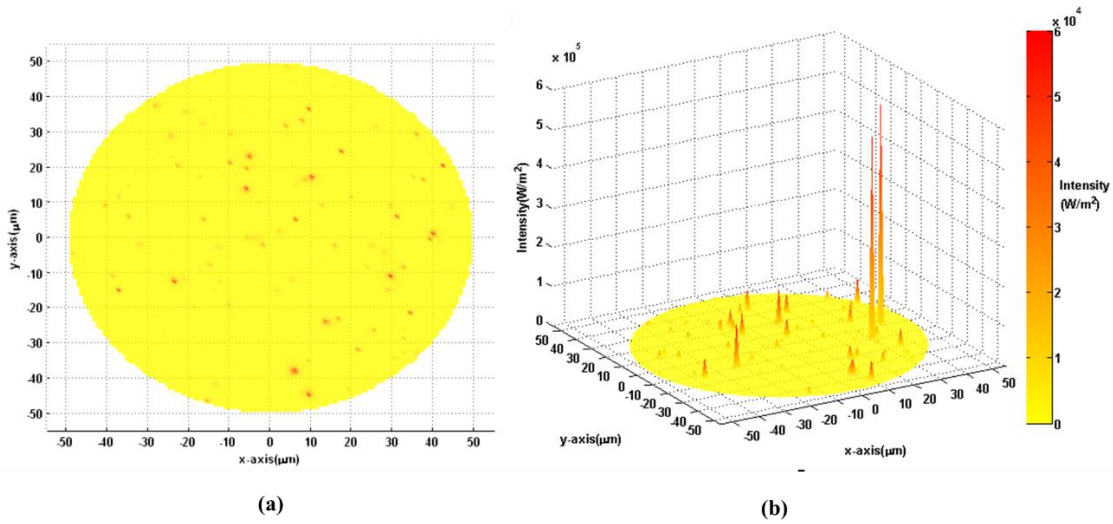
Figure 17. (a) top and (b) tilt views of emitted light intensity distribution from a SSI-LED of 100 μm diameter with 200 randomly distributed nano-resistors at a distance of 80 nm above the dielectric/ITO interface
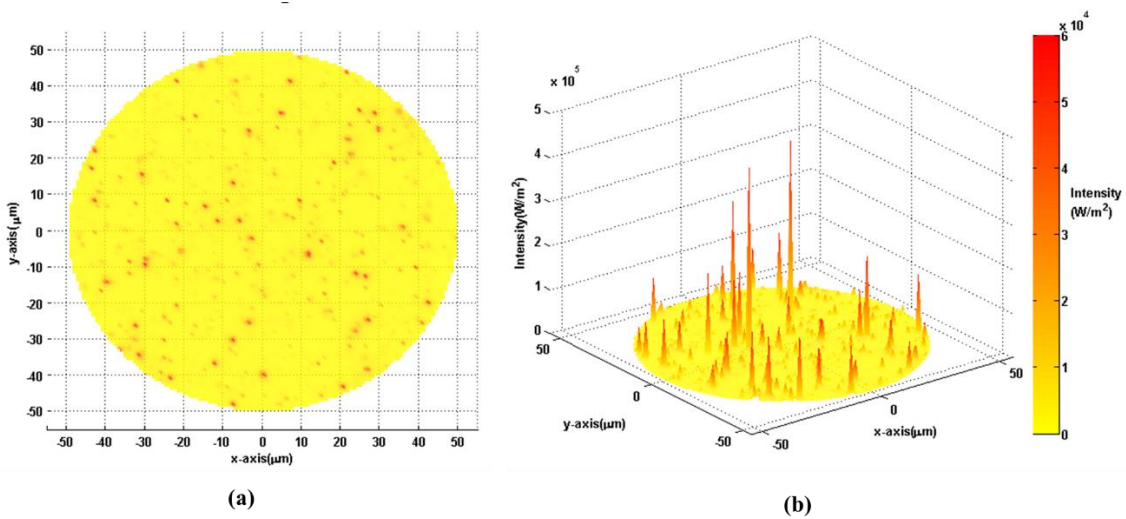
Figure 18. (a) top and (b) tilt views of emitted light intensity distribution from a SSI-LED of 100 μm diameter with 1000 randomly distributed nano-resistors at a distance of 80 nm above the dielectric/ITO interface.

The top view of the emitted light intensity distribution, at a distance of 2 mm from the gate dielectric/ITO interface of the same SSI-LED as that in Fig. 18, is shown in Figure 19(a). No individual bright spots can be observed due to the large distance above the device. Moreover, the center region of the device has the largest light intensity because of the randomly distributed nano-resistors. The decrease in the light intensity from the center towards the edge is symmetrical and similar to the light decay of a single nano-resistor. This is consistent with the Central Limit Theorem in statistical theory, which states that the sum of the independent random variables approaches a normal distribution, i.e., a bell curve, as the sample size (here the number of nano-resistors) becomes larger. Fig. 19(b) shows the 1-D intensity plots for the SSI-LEDs (along the diameter) with increasing number of nano-resistors. The intensity distribution follows a bell curve and is consistent with increasing number of nano-resistors. Moreover, the peak intensity increases with increase in the number of nano-resistors and follows the earlier experimental studies.[25]
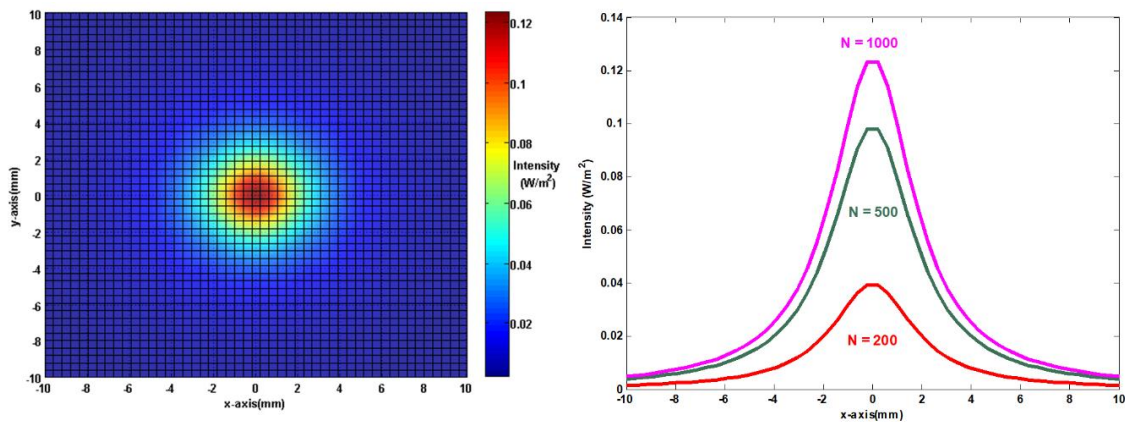
Figure 19. (a) Top view of light intensity distributions at 2 mm distance above the dielectric/ITO interface of the same SSI-LED as in Fig. 3 with 1000 nano-resistors, (b) 1-D intensity plots for 100 µm diameter SSI-LED following normal distribution with increasing number of nano-resistors

The localized geometrical arrangements of the nano-resistors formed in the gate dielectric also affected the shape and intensity distribution observed over individual bright dots at higher magnifications. Figure 20 shows the emitted intensity distribution at a distance of 80 nm from the dielectric/ITO interface for nano-resistors arranged in different geometrical layouts – linear, triangular, square, and face-centered square with the inter-nanoresistor distance of 200 nm. The intensity distribution over the nano-resistor at the center is highest in the linear (Fig. 20(a)) and face-centered square (Fig. 20(d)) layout. All the geometrical layouts show symmetrical intensity distributions.
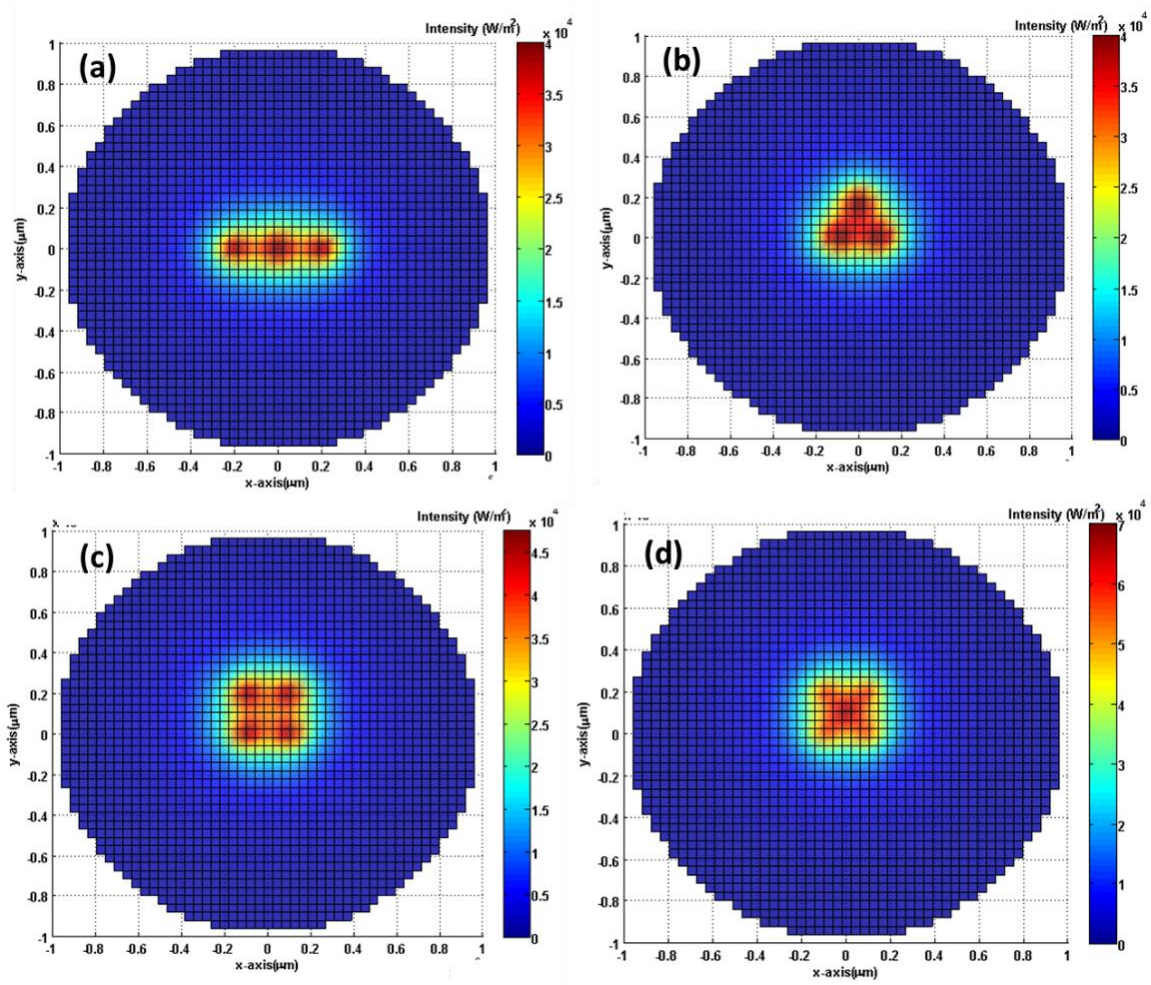
Figure 20. Light intensity from nano-resistors of diameter 20 nm, at a distance of 80 nm from dielectric/ITO interface, arranged in different geometrical layouts – (a) linear (b) triangular (c) square and (d) face centered separated by 200 nm.

Moreover, larger-sized nano-resistors in the vicinity of small-sized nano-resistors resulted in the observation of distorted light intensity distributions. This is shown in Figure 21, where large-sized nano-resistors of diameter 100 nm are present in the vicinity of smaller nano-resistors of diameter 50 nm.

54
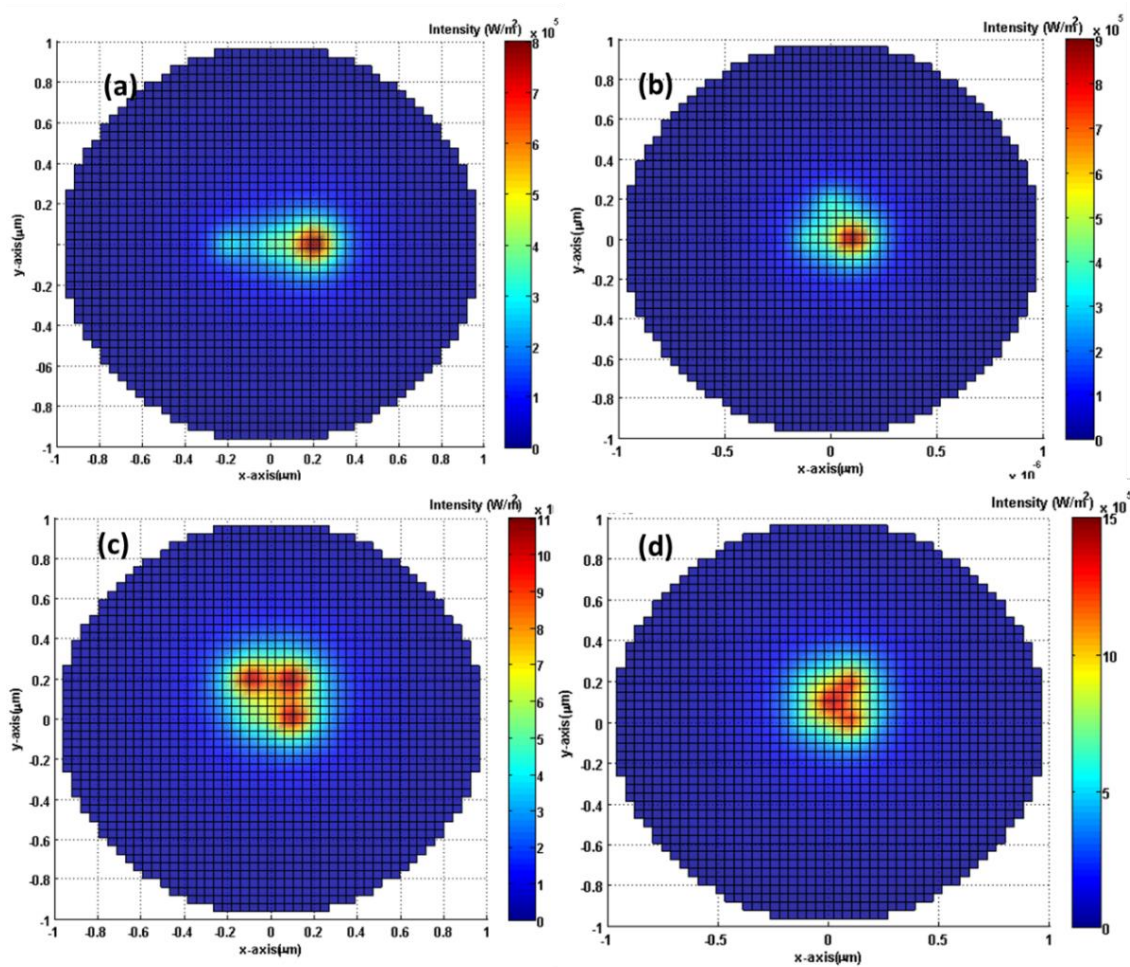
Figure 21. Distorted light intensity distribution seen for different geometrical layouts, as in Fig. 21 except that with the presence of larger sized nano-resistors of diameter 100 nm in the vicinity of smaller sized nano-resistor of diameter 50 nm.

The geometrical layouts used for intensity distribution studies in Fig. 21 are similar to those used in Fig. 20. These arrangements may be associated with different light dot patterns seen in the highly magnified image of an actual SSI-LED shown in Figure 22.[68]

For instance, the intensity distribution in the linear layout of Fig. 20(a) is similar to that observed for linearly formed light dots shown inside red boxes in Fig. 22(b). The triangular intensity distribution observed in Fig. 20(b) is similar to the light dots shown inside blue triangles in Fig. 22(b). Few of the distorted light intensity distributions, like in Fig. 21(a) and (b), can be linked with the warped light dots seen inside the purple ovals shown in Fig. 22(b). Further, the L-shaped light distributions in Fig. 21(c) and (d) is equivalent to the L-shaped light dots arrangement visible in the SSI-LED, as shown in Fig. 22(b).
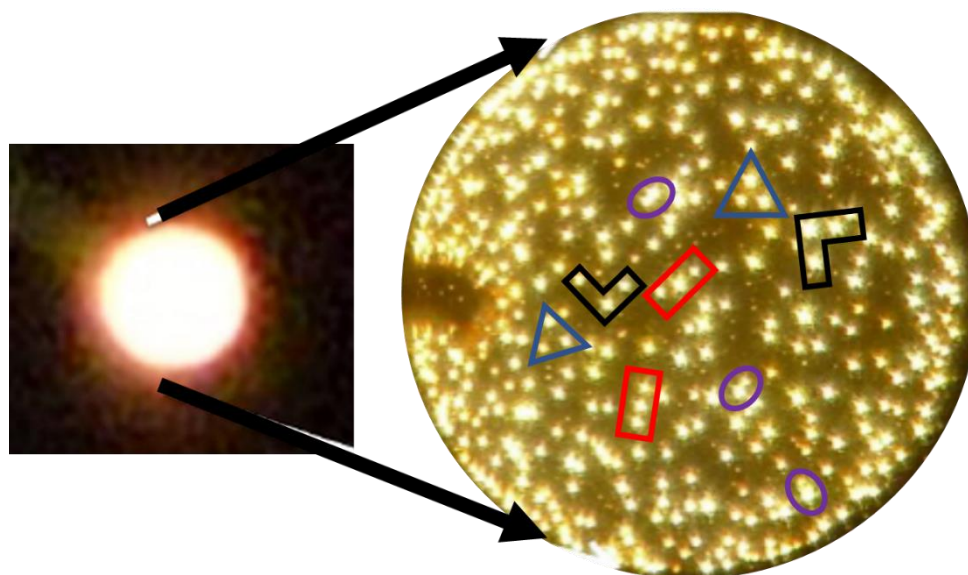
Figure 22. (a) Low and (b) High magnification of WO$_3$ SSI-LED stressed at -20V.[68]

4.4. Summary

In summary, emitted light intensity distribution over the SSI-LED was analytically studied under the assumption that nano-resistors act as blackbody radiators. Fundamental physics-based calculations were performed in order to estimate radiation intensity from SSI-LED. Adjacent nano-resistors formed at considerable distances of about 200 nm were more resolvable at higher magnifications than to those formed at a smaller distance. Cluster formation and the formation of a few large-sized nano-resistors in the gate dielectric were associated with the observation of bright regions seen at higher magnifications. A significant increase in the number of larger bright red spots was reported at higher voltages with a large number of nano-resistors resulting from increased cluster formation and more large-sized nano-resistors. Light from individual nano-resistors could not be resolved at lower magnifications. The SSI-LED was demonstrated as a single light source when viewed from more considerable distances, with the center region of the device being the brightest and light intensity falling uniformly in the radially outwards direction. Shape and intensity distribution observed over individual bright dots at higher magnifications were significantly affected by the local geometrical arrangements of the nano-resistors formed in the gate dielectric.

5. CONCLUSIONS

This thesis mainly investigated the electrothermal and emitted light characteristics of the solid state incandescent light emitting device (SSI-LED) through numerical and analytical computations. The estimation of several physical parameters, such as electrical resistivities and nano-resistor temperature, relied on the experimental data, e.g., J-V_g characteristics reported for the SSI-LED. At times, for materials with unknown behaviour, required properties were either estimated using fundamental physical laws, or relevant assumptions were made.

The Finite Element Method (FEM) in COMSOL Multiphysics software was used to calculate temperature distributions and current density variations in the SSI-LED device. The calculations were more focused in the regions inside nano-resistors and their surrounding media. The temperature estimates were more accurate for optimized boundary conditions based on inferences made from comparison between blackbody radiation and the optical emission spectrum. SEM micrographs showing bump formation, observed in the ITO gate electrode due to localized melting, were confirmed from the high temperatures recorded near the nano-resistor/ITO gate interface. The current density variation near the edge of the large nano-resistors affected the local temperature distribution across the cross-section of nano-resistors. Theoretical calculations of the light filtration effect of ITO and a-Si:H thin films on the emitted light spectrum from the ZrHfO high-k dielectric based SSI-LED are performed. Detailed comparative studies with spectra recorded from actual SSI-LED with the same filters were presented as well. The study speculated that the ITO thin film filter above nano-resistors formed in the dielectric layer

may melt due to intense Joule heating during the passage of a large current. This was further corroborated by the comparison studies reported for the SSI-LED with a-Si thin film filter, where the experimental spectrum more closely fitted with the computed spectrum corresponding to SSI-LED with poly-Si thin film filter. The a-Si film may recrystallize to form poly-Si during operating conditions. The simulated light emission spectra for SSI-LEDs with different thin film filters were characterized using corresponding CCT's and the CIE (x,y) chromaticity diagram. The broadband spectrum emitted from the SSI-LED can be narrowed down with the addition of thin film filters, and the peak of the filtered spectrum depended upon the absorption coefficient of the filter material. Lastly, fundamental physics-based calculations were performed to study the intensity distribution of light emitted from SSI-LED by treating nano-resistors as blackbody radiators. Adjacent nano-resistors formed at considerable distances of about 200 nm were more resolvable at higher magnifications than those formed at a smaller distance. Formation of nano-resistor clusters and a few large nano-resistors in the gate dielectric were associated with the high intensity regions observed at higher magnifications. The SSI-LED acted as a single light source when viewed from farther distances and was equivalent to the low magnification images of SSI-LED, following a bell curve-shaped light intensity distribution. Intensity distribution observed over individual bright dots at higher magnifications were significantly affected by the local geometrical arrangements of the nano-resistors formed in the gate dielectric and could be associated very well with the high magnification images of the actual SSI-LED device.

REFERENCES

[1]   M. Guarnieri, *IEEE Industrial Electronics Magazine*, **9** (3), 44 (2015).

[2]   E. L. Williams, K. Haavisto, J. Li, and G. E. Jabbour, *Adv. Mater.* **19**, 197 (2007).

[3]   J. M. Phillips, M. E. Coltrin, M. H. Crawford, A. J. Fischer, M. R. Krames, R. Mueller-Mach, G. O. Mueller, Y. Ohno, L. E. S. Rohwer, J. A. Simmons, and J. Y. Tsao, *Laser and Photon. Rev.,* **1**, 307 (2007).

[4]   J. Schleich, B. Mills, and E. Dütschke, *Energy Policy,* **72** (2014).

[5]   M. A. Schreuder, K. Xiao, I. N. Ivanov, S. M. Ivanov, S. J. Rosenthal, *Nano Lett.* **10**, 573 (2010).

[6]   N. Holonyak Jr. and S. F. Bevacqua, *Appl. Phys. Lett.,* **1**, 82 (1962).

[7]   T.S. Perry, M. George Craford Biography. *IEEE Spectrum,* **32** (2) (1995).

[8]   S. Kasap, "*pn junction devices and light emitting diodes*," an e-booklet http://www.phy.olemiss.edu/~cremaldi/PHYS417/PNJunctionDevices.pdf.

[9]   B. J. Sealy, *Journal of the Institution of Electronic and Radio Engineers*, **57**, No. 1 (Supplement), (1987).

[10]   G. P. Agrawal and N. K. Dutta, *Semiconductor Lasers, 2nd ed.*, Kluwer Academic Publishers, Massachusetts (2001).

[11]   J. W. Stinson, *U. S. Patent 4*, **992**, 704 (1991).

[12]   S. Nakamura, T. Mukai, and M. Senoh, *Appl. Phys. Lett.*, **64**, 1687–1689 (1994).

[13]   S. Nakamura, M. Senoh, N. Iwasa, S.-I. Nagahama, T. Yamada, and T. Mukai, *J. Appl. Phys.,* **34**, L1332–L1335 (1995).

[14]   J. Cho, J. H. Park, J. K. Kim, and E. F. Schubert, *Laser Photonics Rev.*, **11**, 1600147 (2017).

[15]   K. Bando, Y. Noguchi, K. Sakano, and Y. Shimizu, *Tech. Digest*, Phosphor Res. Soc. 264th meeting, 5– 14 (1996).

[16]   K. Bando, K. Skano, Y. Noguchi, and Y. Shimizu, *J. Light & Vis. Env.*, **22**, 2–5 (1998).

[17]   S. Nakamura and G. Fasol, *The Blue Laser Diode: GaN Based Light Emitters And Lasers* (Springer-Verlag, Berlin, 1997).

[18]   G. Li, W. Wang, W. Yang, Y. Lin, H. Wang, Z. Lin, and S. Zhou, *Rep. Prog. Phys.*, **79** 056501 (2016).

[19]   S. Sadeghi, S. K. Abkenar, C.W. Ow-Yang, and S. Nizamoglu, *Sci Rep*, **9**, 10061 (2019).

[20]   S. Nizamoglu, T. Ozel, E. Sari, and H. V. Demir, *Nanotechnology*, **18**, 065709, (2007).

[21]   Y. Kuo and C.-C. Lin, *Appl. Phys. Lett.*, **102**, 031117 (2013).

[22]   Y. Kuo and C.-C. Lin, *Electrochem. Solid-State Lett.*, **2**, Q59 (2013).

[23]   Y. Kuo and C.-C. Lin, *Solid-State Electron.*, **89**, 120 (2013).

[24]   Y. Kuo, in *2014 IEEE International Electron Devices Meeting (IEDM),* San Francisco, 15-17 December 2014 (IEEE, 2014), pp. 4.7.1-4.7.4.

[25]   C.-C. Lin and Y. Kuo, *J. Solid State Sci. Technol.*, **3**, Q182 (2014).

[26]   C.-C. Lin and Y. Kuo, *J. Vac. Sci. Technol. B*, **32**, 011208 (2014).

[27]   C.-C. Lin and Y. Kuo, *Appl. Phys. Lett.*, **106**, 121107 (2015).

[28]   S. Zhang and Y. Kuo, *ECS Trans.*, **66** (4), 223 (2015).

[29]   S. Zhang and Y. Kuo, *ECS J. Solid State Sci. Technol.*, **7**, R3023 (2018).

[30]   D. MacIsaac, G. Kanner, and G. Anderson, *Phys. Teach.*, **37**, 520 (1999).

[31]   L. L. Liu, X. N. Zhang, B. J. Yu, Y. Y. Lin, and H. Zhang, *Semicond. Sci. Technol.*, **32**, 055009 (2017).

[32]   C.-C. Lin, Y. Kuo, and X. N. Zhang, *ECS Trans.*, **64**, 1 (2015).

[33]   L. Liu, Y. Wang, Y. Lin, X. N. Zhang, and Y. Kuo, *ECS J. Solid State Sci. Technol.*, **9**, 036004 (2020).

[34]   Y. Kuo and S. Zhang, *ECS J. Solid State Sci. and Technol.*, **8** (12) Q223-Q225 (2019).

[35]   S. Zhang and Y. Kuo, *J. Phys. D: Appl. Phys.*, **51** (2018).

[36]   Y. Kuo and S. Zhang, *AVS 63rd Intl. Symp.*, Abst. # 1844, Nov. 11, 2016.

[37]   S. Zhang and Y. Kuo, *ECS J. Solid State Sci. Technol.*, **6**, Q39 (2017).

[38]   S. Zhang and Y. Kuo, *ECS Tran.*, **75**, 17 (2017).

[39]   Y. Kuo, *ECS Trans.*, **69** (12), 23-29 (2015).

[40]   Y. Kuo, *IEEE Trans. Electron Devices*, **62** (11), 3536 (2015).

[41]   S. Zhang and Y. Kuo*, ECS Trans.*, **77** (2), 63 (2017).

[42]   T. Ashida, A. Miyamura, N. Oka, Y. Sato, T. Yagi, N. Taketoshi, T. Baba and Y. Shigesato, *J Appl. Phys.*, **105**, 073709 (2009).

[43]   M. A. Panzer, M. Shandalov, J. A. Rowlette, Y. Oshima, Y. W. Chen and K. E. Goodson, *IEEE Electron Device Lett.*, **30**(12), 1269 (2009).

[44]   E. A. Scott, J. T. Gaskins, S. W. King and P. E. Hopkins, *APL Materials*, **6** (5),
        058302 (2018).

[45]   P. G. Sverdrup, *J. Heat Trans.*, **123**, 130 (2001).

[46]   Y. Kuo, in *22nd International Workshop on Active-Matrix Flatpanel Displays
        and Devices (AM-FPD)*, Kyoto, 1-14 July 2015 (IEEE, 2015), pp. 9-12 (2015)

[47]   M. Haurylau, N. A. Nelson, and E. G. Friedman, *IEEE Journal of Selected
        Topics in Quantum Electronics*, **12**(6), (2006).

[48]   D. A. B. Miller, *Proc. SPIE*, **70**, 80 (1998).

[49]   K. W. Goossen, J. E. Cunningham, W. Y. Jan, and R. Leibenguth, *IEEE J.
        Quantum Elect.*, **34**, 431 (1998).

[50]   Shukla and Y. Kuo, *ECS Trans.*, **97**(2), 69-77 (2020).

[51]   M. Planck, *The Theory of Heat Radiation*, *M. Masius, (transl.) (2nd ed.)* (1914).

[52]   J. Agassi, *Science*, **156**, 3771 (1967).

[53]   J. Zhang, A. C. E. Chia and R. R. LaPierre, *Semicond. Sci. Technol.*, **29**, 054002
        (2014).

[54]   M. Hirose, M. Taniguchi, and Y. Osaka, *J. Appl. Phys.*, **50**, 377 (1979).

[55]   X. Li, C. Zhang, Z. Yang and A. Shang, *Opt. Express*, **21**, A677 (2013).

[56]   M. Perez, C. Santiago, F. Renero, and C. Zuniga, *Opt. Eng.*, **45**, 123802 (2006).

[57]   G. Oh, K. S. Lee, and E. K. Kim, *Current Applied Physics*, **15**, 794 (2015).

[58]   T. Smith and J Guild, *Trans. Opt. Soc.*, **33**, 73 (1931).

[59]   A. Zukauskas, M.S. Shur, and R. Gaska, *Introduction to Solid State Lighting*.
        (Wiley-Interscience, New York: 2002).

[60]   Stefan J, Sitzber. *Math.-Nat.wiss. Cl. kaiserlichen Akad. Wiss.*, **79**, 391 (1879).

[61]   Boltzmann L, *Ann. Phys. Chem.*, **22**, 291 (1884).

[62]   C. H. Tung, K. L. Pey, W. H. Lin, and M. K. Radhakrishnan, *IEEE Electron Device Lett.*, **23**, 526 (2002).

[63]   S. Lombardo, J. H. Stathis, B. P. Linder, K. L. Pey, F. Palumbo, and C. H. Tung, *J. Appl. Phys.*, **98**, 121301 (2005).

[64]   A. Shukla and Y. Kuo, *MRS Adv.*, 1-9 (2020).

[65]   E. A. Scott, J. T. Gaskins, S. W. King, and P. E. Hopkins, *APL Materials*, **6** (5), 058302 (2018).

[66]   G.V. Samsonov, N.F. Podgrushko, and M.I. Lesnaya, *Soviet Physics Journal*, **18**, 1276–1280 (1975).

[67]   N. M. Khusayfan and M. M. El-Nahass, *Adv. in Cond. Matter Phys.*, **2013** (2013).

[68]   C.-C. Lin, *High-K Based Non-Volatile Memory Devices with The Light Emitting Application*, PhD. Dissertation, Texas A&M University, College Station, Texas (2014).

APPENDIX A

COMSOL MULTIPHYSICS

The evolution in computational technology has enabled development of advanced computer software used in the field of science and engineering. The COMSOL Multiphysics is a modeling and simulation software that allows user to solve individual or combination of physics-based problems that can be formulated using partial differential equations (PDEs). In this master's thesis COMSOL 5.2a has been used. The mathematical models for several physical phenomena in the field of electromagnetics, heat transfer, acoustics, structural mechanics, fluid dynamics, chemical reactions, etc. can be developed in 1D, 2D or 3D depending upon the requirements.

COMSOL follows well established numerical technique – Finite Element Method (FEM) implemented using computationally generated mesh schemes to solve the mathematical problems with error control using a variety of numerical solvers. The COMSOL enables user to perform both stationary and time-dependent (transient) analysis, linear and non-linear analysis, etc. In Section 3 of this thesis research, authors focus on solving an electrothermal problem set up in three-dimensional space to obtain stationary solutions using AC/DC, and Heat Transfer modules in COMSOL Multiphysics® 5.2a software package.

Basic problem formulation and simulation steps used in COMSOL for the problem discussed in Section 3 are as follows:

1. Define Problem and Study Type: Time independent, 3-D computational domain, Multiphysics problem (Joule Heating – Heat Transfer and Electric Current)

2. Define and Draw Geometry: See Section 3.2.1

3. Build Mesh: Custom computational mesh based on domain type is defined. See Section 3.2.4 for details

4. Define Physics: Heat Transfer in Solids and Electric Current nodes are added along with a Multiphysics node to account for joule heating

5. Set Solver Parameters: Relative Tolerance = 0.001, Time stepping intermediate

6. Postprocessing

APPENDIX B

C.I.E. COLORIMETRY

Light characteristics corresponding to a light emission spectrum can be described

by properties like CIE chromaticity coordinates, correlated color temperature (CCT), etc.

and are calculated using NIST CQS 7.4 program.[40] The International Commission on

Illumination created color space systems in 1931, CIE 1931 RGB color space and CIE

1931 XYZ color space, to describe all visible colors to an average human eyesight. The

XYZ color space is set of three tristimulus values X, Y, and Z given as follows:

$$X = \int \bar{x}(\lambda)I(\lambda)d\lambda \qquad \text{[A-1a]}$$

$$Y = \int \bar{y}(\lambda)I(\lambda)d\lambda \qquad \text{[A-1b]}$$

$$Z = \int \bar{z}(\lambda)I(\lambda)d\lambda \qquad \text{[A-1c]}$$

where $I(\lambda)$ is the spectral power distribution, and $\bar{x}$, $\bar{y}$, and $\bar{z}$ are the color matching

functions.[41] The three color matching functions shown in Figure 23 are similar to the

spectral sensitivity of the three kinds of cone cells responsible for color sensation in human

eyes with a normal vision. A complete plot of all visible colors in XYZ color space

described above is three-dimensional and is often difficult to demonstrate. However, the

concept of color has two components: brightness and chromaticity. The XYZ color space

is designed such that the Y measures color luminance. Therefore, derived parameters x

and y are used to specify chromaticity and are given as,

$$x = \frac{X}{X+Y+Z} \qquad \text{[A-2a]}$$

$$y = \frac{Y}{X+Y+Z} \qquad \text{[A-2b]}$$

67

$$z = \frac{Z}{X+Y+Z} = 1 - x - y \qquad\qquad\qquad\qquad \text{[A-2c]}$$

The derived color space CIE xyY specified by above parameters x, y, and Y is widely used

to characterize colors.
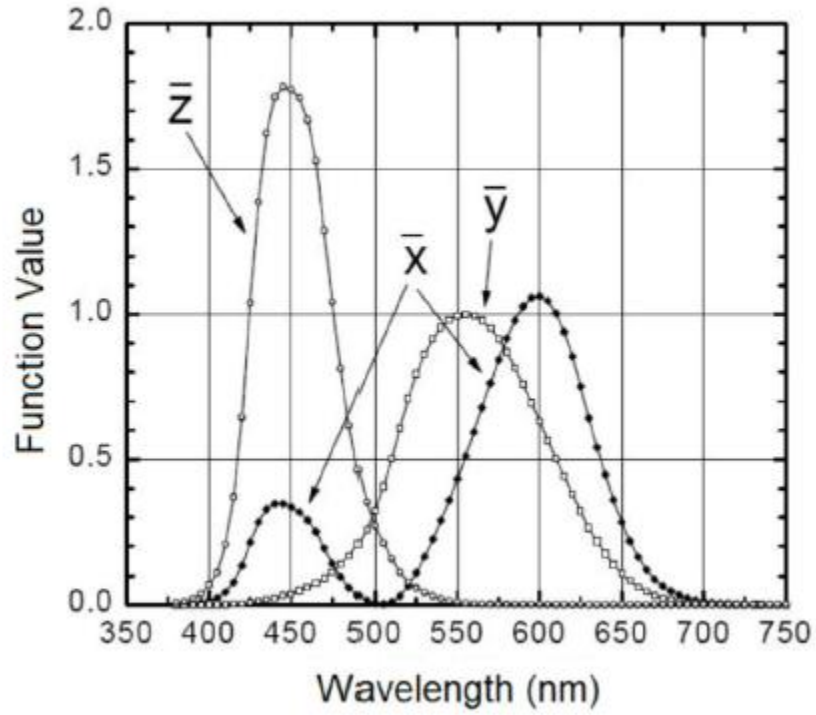
Figure 23. The 1931 CIE color-matching functions. (Reprinted from Ref. 59. Copyright 2002 Wiley.)

APPENDIX C

```matlab
%% calculation of light filtration effect on theoretical spectrum
clc;
clear all;

%% retrieving absorption data and experimental spectrum data
dir = 'a-Si_transmittance_data.xlsx';
dir2= 'ITO_with_a-Si_filter_experimental_data.csv';
dir3 = 'spectrum_ssi_led.csv';
%% data preprocessing
T_data = xlsread(dir,'A:Q');
[nrows,ncol]=size(T_data);
data = [T_data(:,2),T_data(:,7),
T_data(:,9),T_data(:,16),T_data(:,17)];
data(any(isnan(data),2),:) = [];
[nr,nc]=size(data);


%% constants
film_thick= [100E-7]; %in cm
Temp=4000;
lambda=(200:10:1000);
c=3*10^8; % speed of light in vacuum
h=6.625*10.^-34; %  Planck constant
k=1.38*10.^-23; %   Boltzmann constant
C = {[1 0 0],[0 1 0],[1 0 1]}; %color: red green magenta
I1 = (2*h*c.^2)./(((lambda.*1e-
9).^5).*(exp((h.*c)./(k.*Temp.*(lambda.*1e-9)))-1));%absolute spectrum
I1_norm=I1./max(I1); % normalized spectrum

% calculating transmittivity for different thin films
for i=1:2
    data(:,nc+i)=exp(-film_thick*data(:,1+i));

%polyfit transmittivity data, degree of polynomial selected based
fitting parameter R-square
    p(i,:)=polyfit(data(:,1),data(:,nc+i),4);
    t(i,:) = polyval(p(i,:),lambda);
    ylim([0 inf])
    hold on

    plot(lambda,I1_norm.*t(i,:),'LineWidth',3, 'color', C{i});
    hold on
    %extract peak wavelength
    [film_max,idx_film_max]= max(I1_norm.*t(i,:))
    f_peak_lambda(i)=lambda(idx_film_max);
end


%%theoretical spectrum after ITO filtration
ITO_t_calc=exp(-film_thick*data(:,5));
p_ITO=polyfit(data(:,4),ITO_t_calc,4);
```

```matlab
T_ITO = polyval(p_ITO,lambda);
plot(lambda,I1_norm.*T_ITO,'LineWidth',3, 'color', C{3});
[ITO_max,idx_ITO_max]= max(I1_norm.*T_ITO)
ITO_peak_lambda = lambda(idx_ITO_max);
hold on

%% spectrum a-Si_filter_experimental_data and ssi_led spect

exp_data= xlsread(dir2,'A:C');
plot(exp_data(:,1),exp_data(:,3),'LineWidth',3,'color','b');
hold on
title('thin film filter (thickness = 100 nm)');
xlabel('wavelength( \lambda )');
ylabel('Normalized intensity');
```

APPENDIX D

```matlab
%% generating N nanoresistor coordinates
clc
clear all
N=1000; %number of points
n=1;  %counter
%simulation cube
x_range=[-100 100]*1E-6; %Range of width in x
y_range=[-100 100]*1E-6; %Range of width in y
z_range=[0]; %Range of width in z
centre=[mean(x_range),mean(y_range),mean(z_range)]; %Center of
simulation box
radius=50E-6; %Radius of circular gate
NR_point_arr=zeros(N,3); %Array to store Random co-ordinates
L=200E-9;% fixed distance b/w two NRs
rng(0) %random seed value;
while n<=N
    %Generate 2 random numbers for x and y coordinates
    temp_xy = (y_range(2)-y_range(1)).*rand(1,2) + y_range(1);
    temp_xyz = [temp_xy,0];
    dist = pdist([temp_xyz;centre],'euclidean'); %Find distance between
the point generated and the center of simulation box

    for q=1:n

      pairwise_d(q,:)=pdist([temp_xyz;NR_point_arr(q,:)],'euclidean');
    end
    check = pairwise_d(:,1)>L;
    if dist<radius && sum(check)== n  %discard if distance less than
radius or distance b/w two points is less than L
        NR_point_arr(n,:)=temp_xyz;
        n=n+1;
    end
end
%%

%%random co-ordinates distribution 2D plot
figure
scatter(NR_point_arr(:,1),NR_point_arr(:,2),'.')
xlim([-55 55]*1E-6);
ylim([-55 55]*1E-6);
axis square
hold on;
viscircles([mean(x_range),mean(y_range)],radius,'EdgeColor','k');
xlabel('x-axis (m)');
ylabel('y-axis (m)');

%%defining constants
e=1;
sigma= 5.67E-8;  %stefan boltzman constant W m-2 K-4
r1= 50E-9; %large 100 nm dia
```

71

```matlab
r2 = 25E-9; %medium 50 nm dia
r3 = 10E-9; %small 20 nm dia
T1=4000;% temp of each nanoresistor
T2=4000;
T3=4000;%K
Tc=298; % surrounding temperature K
d= [2E-3];  %screen distance
c=3*10^8; % speed of light in vaccum
h=6.625*10.^-34; %  Planck constant
k_boltz=1.38*10.^-23; %   Boltzmann constant
alpha = 0.058E5; %ITO absorption coefficient cm-1
ITO_film_thickness = 80E-6; % in cm

P1= e*(pi*r1.^2)*sigma*(T1.^4-Tc.^4);%power emitted from each NR source
P2= e*(pi*r2.^2)*sigma*(T2.^4-Tc.^4);
P3= e*(pi*r3.^2)*sigma*(T3.^4-Tc.^4);

%%Resultant Intensity Calculation
X=linspace(-10E-3,10E-3,50);
Y=linspace(-10E-3,10E-3,50);
Z=d;
P=zeros();% grid matrix to store resultant intensity recorded at each
cell
for i=1:length(X)
    for j=1:length(Y)
        I=0;
        for k=1:length(NR_point_arr) %k=Nanoresistor count
            r=sqrt((X(i)-NR_point_arr(k,1)).^2+(Y(j)-
NR_point_arr(k,2)).^2+(Z-NR_point_arr(k,3)).^2);%r=distance of gridcell
from source
            if k<(length(NR_point_arr)*0.05)
                test=P1./(4*pi*r.^2);
            end
            if k>(length(NR_point_arr)*0.05)&&
k<(length(NR_point_arr)*0.3)
                test=P2./(4*pi*r.^2);
            end
            if k>(length(NR_point_arr)*0.3)
                 test=P3./(4*pi*r.^2);
            end
            I=I+ test;
        end
        P(i,j)=I;
    end
end
P=P.*exp(-alpha.*ITO_film_thickness);

%%Intensity distribution surface plot
[xx,yy] = meshgrid(X,Y); % transfer into 2D array
P((xx.^2 + yy.^2) >= (radius)^2) = NaN; % set values outside the circle
to be NaN
figure
s = surf(X,Y,P,'EdgeColor','k','FaceColor','interp','FaceAlpha',0.8);
```

```matlab
xlim([-10E-3 10E-3]);%adjusted based on plot requirements
ylim([-10E-3 10E-3]);
xlabel('x-axis(mm)','fontweight','bold','fontsize',10);
ylabel('y-axis(mm)','fontweight','bold','fontsize',10);
zlabel('Intensity(W/m^2)','fontweight','bold','fontsize',10);
h = colorbar;
set(get(h,'title'),'string','Intensity (W/m^2)');
caxis([0 0.04]) % colorbar scale
colormap(flipud(autumn)) % custom colormap
view(0,90);
```